

and four θ_D angles decrease by $\Delta\theta_D$. In addition four ϕ_A angles decrease by $\Delta\phi_A$ and four θ_A angles increase by $\Delta\theta_A$ to θ^* . From these considerations eq A4 and A5 are obtained with, as above, a single bending force constant assumed for both L-M-L and H-M-L bending:

$$2V_{AD} = 4h_A(1 + g_A^2)\Delta\theta_A^2 + 4h_D(1 + 2g_D^2)\Delta\theta_D^2 \quad (\text{A4})$$

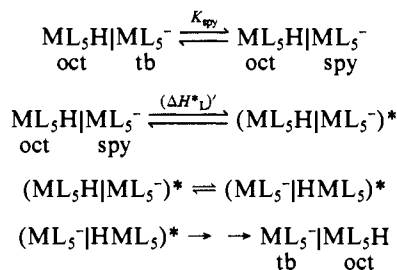
$$\theta^* = \frac{4h_A(1 + g_A^2)\theta_A^0 + 4h_D(1 + 2g_D^2)\theta_D^0}{4h_A(1 + g_A^2) + 4h_D(1 + 2g_D^2)} \quad (\text{A5})$$

(2) **Pathways Involving Fluxional Species.** Rather detailed knowledge of the potential-energy surface for pseudorotation is required if this fluxional feature is to be incorporated into the model correctly. The following questions arise: (1) Is the square-pyramidal ML_5^- form (in which the axial/equatorial identity is lost) an intermediate or a transition state? If the square-pyramidal species is an intermediate, a pre-equilibrium step (K_{spy} ; $\Delta H^\circ_{\text{spy}}$) to give this species can be incorporated in the mechanistic scheme. (2) What are the angles in the square-pyramidal form? If the trans L-M-L basal angle is 180° the square-pyramidal form is perfectly matched to an octahedral hydride and no further deformation is required. However, the trans basal angle is generally $<180^\circ$ in d^8 structures which have been characterized. (3) Provided that the trans basal angle of the square-pyramidal ML_5^- species is known, how is the geometry difference between this form ($\text{spy-}ML_5^-$) and the octahedral HML_5 to be taken into account? Flattening of the square pyramid to a basal angle of 180° could be as facile as the Berry motion; that is, the effective bending force constant could be quite small, perhaps $0.01 \text{ mdyn } \text{\AA} \text{ rad}^{-2}$. In such a situation the proton exchange would occur through transfer from the hydride in its equilibrium geometry to a base having the hydride's spectator ligand geometry, with ΔH^*_L reflecting only the cost of geometric

rearrangement on the base ML_5^- . On the other hand, the force constant for flattening of the square pyramid which effects the pseudorotation need not be as small as for the Berry motion; Hoffman's surface for PH_5^{40} indicates that such a motion is harmonic and energetic, with the bending force constant perpendicular to the pseudorotation deformation being ~ 30 times greater than along the pseudorotation deformation. In such a case, knowledge of the geometry of $\text{spy-}ML_5^-$ is critical.

For the sake of discussion, one specific set of constraints is considered. These are illustrated in Scheme IV. The rear-

Scheme IV



angement of the base ML_5^- is treated as a rapid pre-equilibrium (K_{spy}) and proton exchange is taken to occur between the open apical site on square-pyramidal ML_5^- , $\text{spy-}ML_5^-$, and rigid octahedral ML_5H with ΔH^*_L determined by $\Delta H^\circ_{\text{spy}}$ and $(\Delta H^*_L)'$ arising from the ca. 8° out-of-plane bend required for $\text{spy-}ML_5^-$ and HML_5 angles. From the bending force constant estimate³⁴ $0.6 \text{ mdyn } \text{\AA} \text{ rad}^{-2}$ and eq A4 and A5 $(\Delta H^*_L)'$ contributes $\sim 4 \text{ kcal mol}^{-1}$ to ΔH^* . With $K_{\text{spy}} \simeq 0.2$, requirements for angular reorganization reduce the ML_5H/ML_5^- exchange rate by a factor of 5×10^3 at 298 K, with a total contribution of $\sim 5 \text{ kcal mol}^{-1}$ to ΔH^* .

Synthesis, Structure, Dynamic Behavior, and Reactivity of Rhenium Phosphido Complexes $(\eta^5\text{-C}_5\text{H}_5)\text{Re}(\text{NO})(\text{PPh}_3)(\text{PR}_2)$: The "Gauche Effect" in Transition-Metal Chemistry

William E. Buhro, Bill D. Zwick, Savas Georgiou, John P. Hutchinson, and J. A. Gladysz*

Contribution from the Department of Chemistry, University of Utah, Salt Lake City, Utah 84112. Received August 31, 1987

Abstract: Reactions of $(\eta^5\text{-C}_5\text{H}_5)\text{Re}(\text{NO})(\text{PPh}_3)(\text{X})$ ($\text{X} = \text{OTs}$ ($\text{OSO}_2\text{-}p\text{-Tol}$), OTf (OSO_2CF_3)) with PR_2H ($\text{R} = \text{Ph}$ (**a**), $p\text{-Tol}$ (**b**), Et (**c**), $t\text{-Bu}$ (**d**)) give secondary phosphine complexes $[(\eta^5\text{-C}_5\text{H}_5)\text{Re}(\text{NO})(\text{PPh}_3)(\text{PR}_2\text{H})]^+\text{X}^-$ (**2a-TsO**⁻, **2b-TsO**⁻, **2c-TfO**⁻, **2d-TfO**⁻; 87–96%). Reactions of **2a-d-X**⁻ with $t\text{-BuO}^-\text{K}^+$ give phosphido complexes $(\eta^5\text{-C}_5\text{H}_5)\text{Re}(\text{NO})(\text{PPh}_3)(\text{PR}_2)$ (**4a-d**; 79–99%). Optically active, configurationally stable (+)-(*S*)-**4b** is analogously prepared. NMR experiments show **4a-d** to have very low PR_2 phosphorus inversion barriers (12.6–14.9 kcal/mol). The rapid alkylation of **4a** by CH_2Cl_2 to give $[(\eta^5\text{-C}_5\text{H}_5)\text{Re}(\text{NO})(\text{PPh}_3)(\text{PPh}_2\text{CH}_2\text{Cl})]^+\text{Cl}^-$ (79%) shows the PR_2 phosphorus to be highly nucleophilic, and **4a** and **4d** are easily oxidized (O_2 , PhIO) to phosphine oxides $(\eta^5\text{-C}_5\text{H}_5)\text{Re}(\text{NO})(\text{PPh}_3)(\text{P}(\text{=O})\text{R}_2)$ (34–60%). The X-ray crystal structures of **4a** and **4d** show that the PR_2 phosphorus lone pairs make 59–60° torsion angles with the rhenium d orbital HOMO. It is proposed that avoided overlap between these orbitals ("gauche effect") is an important Re-PR_2 conformation-determining factor. This proposal is supported by extended-Hückel MO calculations on the model compound $(\eta^5\text{-C}_5\text{H}_5)\text{Re}(\text{NO})(\text{PH}_3)(\text{PH}_2)$.

As exemplified by the classic Dewar–Chatt–Duncanson model for transition metal–olefin complexes,¹ bonds between transition metals and unsaturated ligands commonly consist of two components: (1) donation of ligand electrons to metal σ -acceptor

orbitals, and (2) donation of metal d electrons to ligand π -acceptor orbitals. These interactions are shown schematically in Figure 1. The latter, generally termed back-bonding,^{2,3} has important

(1) (a) Dewar, M. J. S. *Bull. Soc. Chim. Fr.* 1951, 18, C71. (b) Chatt, J.; Duncanson, L. A. *J. Chem. Soc.* 1953, 2939.

(2) Collman, J. P.; Hegedus, L. S.; Norton, J. R.; Finke, R. G. *Principles and Applications of Organotransition Metal Chemistry*; University Science Books: Mill Valley, CA, 1987; pp 37–54.

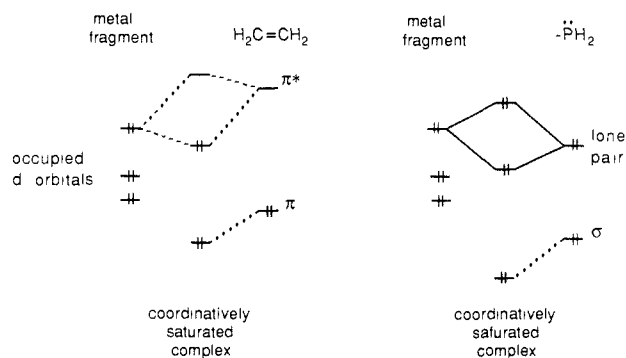
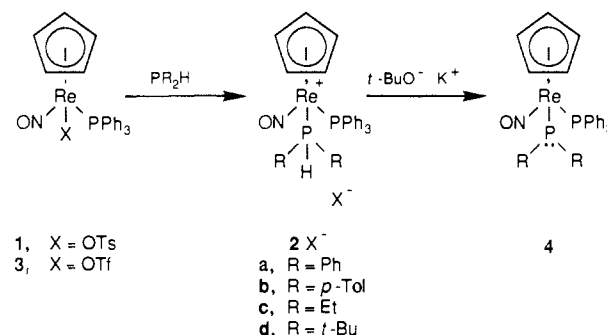


Figure 1. Qualitative comparison of frontier MO interactions in metal alkene and metal phosphido complexes.

consequences for metal–ligand and intraligand bond distances as well as interatomic force constants and is therefore an important determinant of observable structural and spectroscopic properties. Numerous theoretical studies have shown that donor–acceptor overlap between a metal-fragment HOMO and a ligand LUMO is highly dependent upon ligand conformation, thus emphasizing the stereoelectronic nature of back-bonding.^{4–6}

It seemed to us that an equally important stereoelectronic effect should arise when ligands bear donor orbitals instead of acceptor orbitals (Figure 1).⁷ Avoided overlap between the adjacent metal- and ligand-donor orbitals would then be an important conformation-determining factor. In organic and main-group inorganic compounds this is commonly called the “gauche effect”^{8,9} and exerts a profound influence on physical^{8,10,11} and chemical¹² properties. Although this idea is simple and obvious, we were unaware of any studies specifically designed to identify a transition-metal “gauche effect”.⁷ Hence, we sought an appropriate

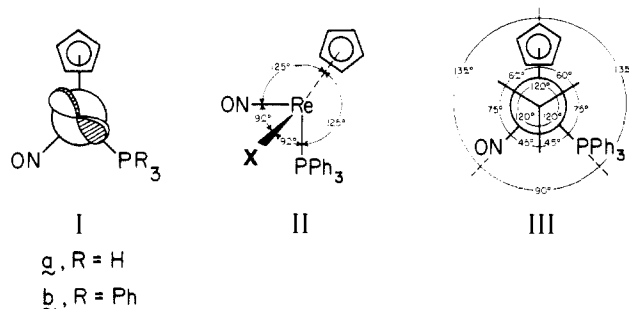
Scheme I. Synthesis of Rhenium Phosphine and Phosphido Complexes



system to probe for this phenomenon.

Transition-metal terminal-phosphido complexes, L_nM–P̄R₂, have been known for some time and their chemistry has attracted much recent attention.^{13–15} Such complexes can have either pyramidal or trigonal-planar phosphorus atoms, depending upon the electronic requirements of the L_nM moiety. The planar geometry is encountered with coordinatively unsaturated metal fragments, where the phosphido ligand lone pair can be delocalized to a low-lying acceptor orbital on the metal. Hence, we sought to study pyramidal phosphido complexes of coordinatively saturated metals, where the phosphido ligand lone pair should remain nonbonding.

We also required a metal fragment with a stereochemically well-defined “lone pair”. The HOMO of the rhenium fragment [(η⁵-C₅H₅)Re(NO)(PPh₃)]⁺, shown in Ib, is a nonbonding d-type



orbital that is well separated from other occupied orbitals.¹⁶ The

(3) Cotton, F. A.; Wilkinson, G. *Advanced Inorganic Chemistry*, 4 ed.; Wiley-Interscience: New York, 1980; pp 81–106.

(4) (a) Albright, T. A.; Hoffmann, P.; Hoffmann, R. *J. Am. Chem. Soc.* **1977**, *99*, 7546. (b) Schilling, B. E. R.; Hoffmann, R.; Lichtenberger, D. L. *Ibid.* **1979**, *101*, 585. (c) Schilling, B. E. R.; Hoffmann, R.; Faller, J. W. *Ibid.* **1979**, *101*, 592. (d) Albright, T. A.; Hoffmann, R.; Thiabeault, J. C.; Thorn, D. L. *Ibid.* **1979**, *101*, 3801. (e) Albright, T. A.; Hoffmann, R.; Tse, Y.; D'Ottavio, T. *Ibid.* **1979**, *101*, 3812.

(5) (a) Kostić, N. M.; Fenske, R. F. *J. Am. Chem. Soc.* **1982**, *104*, 3879. (b) Kostić, N. M.; Fenske, R. F. *Organometallics* **1982**, *1*, 974.

(6) Francl, M. M.; Pietro, W. J.; Hout, R. F., Jr.; Hehre, W. J. *Organometallics* **1983**, *2*, 815.

(7) This paper is specifically concerned with the case where low-lying ligand acceptor orbitals are absent. The complicated situation that arises when ligand acceptor orbitals are also present (as in vinyl ligands, –CH=CHR) has been analyzed by Fenske and Kostić.^{5b} The possibility of metal fragment HOMO/heteroatom donor orbital interactions has been briefly considered previously. See ref 10 and: (a) Kubáček, P.; Hoffmann, R.; Havlas, Z. *Organometallics* **1982**, *1*, 180 (see p 186). (b) Murray, S. G.; Hartley, F. R. *Chem. Rev.* **1981**, *81*, 365. (c) Chisholm, M. H.; Clark, D. L. *Comments Inorg. Chem.* **1987**, *6*, 23. (d) Ashby, M. T.; Enemark, J. H.; Lichtenberger, D. L. *Inorg. Chem.* **1988**, *27*, 191.

(8) (a) Wolfe, S. *Acc. Chem. Res.* **1972**, *5*, 102. (b) Radom, L.; Hehre, W. J.; Pople, J. A. *J. Am. Chem. Soc.* **1972**, *94*, 2371. (c) Epiotis, N. D. *Ibid.* **1973**, *95*, 3087. (d) Bingham, R. C. *Ibid.* **1975**, *97*, 6743. (e) Nelsen, S. F. *Acc. Chem. Res.* **1978**, *11*, 14. (f) Cowley, A. H.; Mitchell, D. J.; Whangbo, M.-H.; Wolfe, S. *J. Am. Chem. Soc.* **1979**, *101*, 5224. (g) Schmidbauer, H.; Deschler, U.; Milewski-Mahrla, B. *Chem. Ber.* **1983**, *116*, 1393. (h) Schmidbauer, H.; Milewski-Mahrla, B.; Müller, G.; Krüger, C. *Organometallics* **1984**, *3*, 38. (i) Jennings, W. B.; Rutherford, M. *Tetrahedron Lett.* **1984**, *25*, 3131. (j) Rauk, A. *J. Am. Chem. Soc.* **1984**, *106*, 6517.

(9) It should be noted that other factors, such as n → σ* interactions, can contribute to the “gauche effect”.⁸ These are not considered in the first-order treatment in this paper.

(10) Jolly, W. L. *Acc. Chem. Res.* **1983**, *16*, 370.

(11) Ogawa, K.; Takeuchi, Y.; Suzuki, H.; Nomura, Y. *J. Am. Chem. Soc.* **1984**, *106*, 831.

(12) See, inter alia: (a) Buncl, E.; Hoz, S. *Tetrahedron Lett.* **1983**, *24*, 4777. (b) Dupuy, C. H.; Della, E. W.; Filley, J.; Grabowski, J. J.; Bierbaum, V. M. *J. Am. Chem. Soc.* **1983**, *105*, 2481. (c) Taira, K.; Mock, W. L.; Gorenstein, D. G. *J. Am. Chem. Soc.* **1984**, *106*, 7831. (d) Deslongchamps, P. *Stereoelectronic Effects in Organic Chemistry*; Pergamon: New York, 1983. (e) Hudson, R. F.; Hansell, D. P.; Wolfe, S.; Mitchell, D. J. *J. Chem. Soc., Chem. Commun.* **1985**, 1406. (f) Buncl, E.; Um, I.-H. *Ibid.* **1986**, 595. (g) Moss, R. A.; Swarup, S.; Ganguli, S. *Ibid.* **1987**, 860. (h) Evansek, J. D.; Blake, J. F.; Jorgensen, W. L. *J. Am. Chem. Soc.* **1987**, *109*, 2349.

(13) Structurally characterized pyramidal terminal phosphido complexes: (a) Barrow, M. J.; Sim, G. A. *J. Chem. Soc., Dalton Trans.* **1975**, 291. (b) Ebsworth, E. A. V.; Gould, R. O.; McManus, N. T.; Pilkington, N. J.; Rankin, D. W. H. *Ibid.* **1984**, 2561. (c) Hutchins, L. D.; Duesler, E. N.; Paine, R. T. *Organometallics* **1982**, *1*, 1254. (d) Baker, R. T.; Whitney, J. F.; Wreford, S. S. *Ibid.* **1983**, *2*, 1049. (e) Weber, L.; Reizig, K.; Boese, R. *Chem. Ber.* **1985**, *118*, 1193. (f) Wroblewski, D. A.; Ryan, R. R.; Wasserman, H. J.; Salazar, K. V.; Paine, R. T.; Moody, D. C. *Organometallics* **1986**, *5*, 90. (g) Bohle, D. S.; Jones, T. C.; Rickard, C. E. F.; Roper, W. R. *Ibid.* **1986**, *5*, 1612. (h) Buhro, W. E.; Chisholm, M. H.; Foltz, K.; Huffman, J. C. *J. Am. Chem. Soc.* **1987**, *109*, 905.

(14) Other key references to the extensive literature on pyramidal terminal phosphido complexes: (a) Cooke, M.; Green, M.; Kirkpatrick, D. *J. Chem. Soc. A* **1968**, 1507. (b) Treichel, P. M.; Dean, W. K.; Douglas, W. M. *J. Organomet. Chem.* **1972**, *42*, 145. (c) Schunn, R. A. *Inorg. Chem.* **1973**, *12*, 1573. (d) Dobbie, R. C.; Mason, P. R. *J. Chem. Soc., Dalton Trans.* **1973**, 1124. (e) Schäfer, H. Z. *Anorg. Allg. Chem.* **1979**, *459*, 157. (f) Malisch, W.; Maisch, R.; Colquhoun, I. J.; McFarlane, W. J. *Organomet. Chem.* **1981**, *220*, C1. (g) Wade, S. R.; Wallbridge, M. G. H.; Willey, G. R. *J. Chem. Soc., Dalton Trans.* **1983**, 2555. (h) Malisch, W.; Maisch, R.; Meyer, A.; Greisinger, D.; Gross, E.; Colquhoun, I. J.; McFarlane, W. *Phosphorus Sulfur* **1983**, *18*, 299. (i) Angerer, W.; Sheldrick, W. S.; Malisch, W. *Chem. Ber.* **1985**, *118*, 1261. (j) Ebsworth, E. A. V.; Mayo, R. *Angew. Chem., Int. Ed. Engl.* **1985**, *24*, 68. (k) Bohle, D. S.; Roper, W. R. *Organometallics* **1986**, *5*, 1607. (l) Ashby, M. T.; Enemark, J. H. *Ibid.* **1987**, *6*, 1323. (m) Crisp, G. T.; Salem, G.; Stephens, F. S.; Wild, S. B. *J. Chem. Soc., Chem. Commun.* **1987**, 600. (n) Fryzuk, M. D.; Bhangu, K. *J. Am. Chem. Soc.* **1988**, *110*, 961.

(15) Jones, R. A.; Seeberger, M. H. *J. Chem. Soc., Chem. Commun.* **1985**, 373.

(16) (a) Kiel, W. A.; Lin, G.-Y.; Constable, A. G.; McCormick, F. B.; Strouse, C. E.; Eisenstein, O.; Gladysz, J. A. *J. Am. Chem. Soc.* **1982**, *104*, 4865. (b) Georgiou, S.; Gladysz, J. A. *Tetrahedron* **1986**, *42*, 1109.

strong directive capacity of this HOMO is evident in complexes of unsaturated ligands such as $-\text{C}(\text{R})=\text{O}$,¹⁷ $=\text{C}(\text{H})\text{C}_6\text{H}_5$,^{16a} and $\eta^2\text{-R}(\text{H})\text{C}=\text{O}$.¹⁸ In each case, the ligand adopts a conformation that maximizes overlap of the rhenium-fragment HOMO with the ligand LUMO. Other relevant geometric features are summarized in formulas II and III. Hence, we set out to synthesize and study the ligand properties of terminal phosphido complexes of the formula $(\eta^5\text{-C}_5\text{H}_5)\text{Re}(\text{NO})(\text{PPh}_3)(\text{PR}_2)$, as detailed below. Portions of this work have been communicated.¹⁹

Results

1. Syntheses of Phosphido Complexes. Reaction of tosylate complex $(\eta^5\text{-C}_5\text{H}_5)\text{Re}(\text{NO})(\text{PPh}_3)(\text{OTs})$ (**1**)^{20,21} with diphenylphosphine, PPh_2H (CH_2Cl_2 , 25 °C, 2 days), gave secondary phosphine complex $[(\eta^5\text{-C}_5\text{H}_5)\text{Re}(\text{NO})(\text{PPh}_3)(\text{PPh}_2\text{H})]^+\text{TsO}^-$ (**2a-TsO**⁻) in 94% yield after workup (Scheme I). Similar reaction of **1** with di(*p*-tolyl)phosphine, $\text{P}(\textit{p}\text{-Tol})_2\text{H}$, gave secondary phosphine complex $[(\eta^5\text{-C}_5\text{H}_5)\text{Re}(\text{NO})(\text{PPh}_3)(\text{P}(\textit{p}\text{-Tol})_2\text{H})]^+\text{TsO}^-$ (**2b-TsO**⁻, 96%).

Reactions of tosylate complex **1** with bulkier phosphines were considerably slower. However, treatment of the more reactive triflate complex $(\eta^5\text{-C}_5\text{H}_5)\text{Re}(\text{NO})(\text{PPh}_3)(\text{OTf})$ (**3**)^{20,21} with diethylphosphine, PEt_2H (benzene, 4 h), and the very bulky di(*tert*-butyl)phosphine, $\text{P}(\textit{t}\text{-Bu})_2\text{H}$ (refluxing benzene, 24 h), gave secondary phosphine complexes $[(\eta^5\text{-C}_5\text{H}_5)\text{Re}(\text{NO})(\text{PPh}_3)(\text{PEt}_2\text{H})]^+\text{TfO}^-$ (**2c-TfO**⁻, 90%) and $[(\eta^5\text{-C}_5\text{H}_5)\text{Re}(\text{NO})(\text{PPh}_3)(\text{P}(\textit{t}\text{-Bu})_2\text{H})]^+\text{TfO}^-$ (**2d-TfO**⁻, 84%), respectively.

Secondary phosphine complexes **2a-d-X**⁻ were characterized by microanalysis (Experimental Section) and IR and NMR (¹H, ¹³C, and ³¹P) spectroscopy (Table I). The ³¹P{¹H} NMR spectra displayed AX patterns characteristic of scalar-coupled PPh_3 and PR_2H ligands. Both ¹H and ³¹P NMR spectra exhibited large diagnostic one-bond J_{PH} (358–397 Hz). Also, IR spectra showed the expected $\nu_{\text{P-H}}$ (2292–2326 cm^{-1}).

The phosphorus–hydrogen bonds of coordinated secondary phosphines are generally quite acidic.^{13g,14j,m,22} Hence, complexes **2a-d-X**⁻ were treated with *t*-BuO⁻K⁺ (THF, 25 °C). This gave air-sensitive phosphido complexes $(\eta^5\text{-C}_5\text{H}_5)\text{Re}(\text{NO})(\text{PPh}_3)(\text{PR}_2)$ (**4a-d**; Scheme I) in 79–99% yields.

Complexes **4a-d** were characterized as described for **2a-d-X**⁻ above (Table I). The IR $\nu_{\text{N}=\text{O}}$ and ¹H and ¹³C NMR $\eta^5\text{-C}_5\text{H}_5$ chemical shifts were diagnostic of neutral $(\eta^5\text{-C}_5\text{H}_5)\text{Re}(\text{NO})(\text{PPh}_3)(\text{X})$ complexes.^{16a,17,20} The phosphido ligand ³¹P NMR chemical shifts in **4a-c** (–46 to –51 ppm) were within a range typical for organophosphines²³ and close to those reported for $(\eta^5\text{-C}_5\text{H}_5)\text{M}(\text{CO})_2(\text{L})(\text{PPh}_2)$ (M = Mo, W).^{14f} The strikingly different di(*tert*-butyl)phosphido ligand ³¹P NMR chemical shift in **4d** (8.58 ppm) parallels trends found with bulky organophosphines.²³ The temperature dependence of some of the NMR data for **4a-d** (Table I) is analyzed below. The UV/visible spectra of **4a**, **4c**, and **4d** showed long tails into the visible, with peaks and shoulders characteristic of phenyl rings (Experimental Section). Complexes **4c** and **4d** exhibited fewer shoulders. Those in **4d** (deep red) were red-shifted relative those in **4c** (deep orange), and ϵ at 400 nm was 1.8 times greater for **4d**.

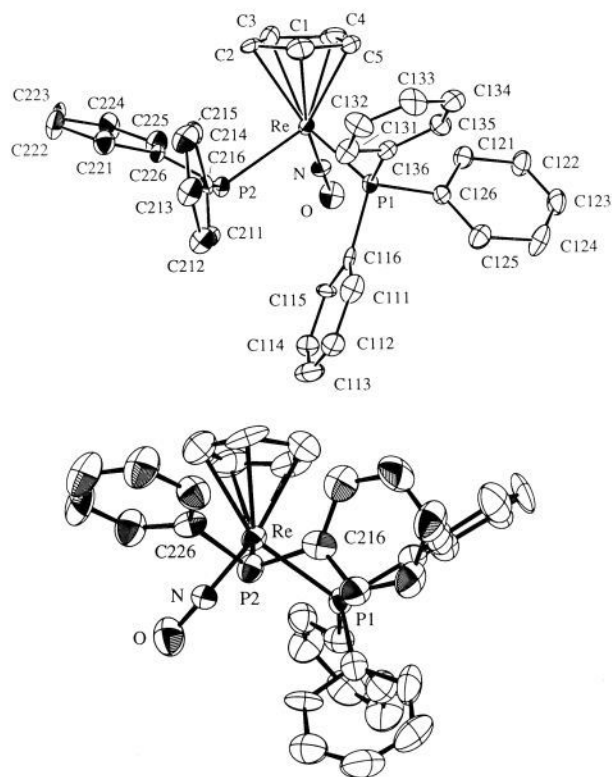


Figure 2. Two views of the molecular structure of $(\eta^5\text{-C}_5\text{H}_5)\text{Re}(\text{NO})(\text{PPh}_3)(\text{PPh}_2)$ (**4a**).

Optically active tosylate complex $(-)(S)\text{-1}$ ^{20,24} was treated with $\text{P}(\textit{p}\text{-Tol})_2\text{H}$ as in Scheme I. This gave secondary phosphine complex $(-)(S)\text{-2b}$ (82%) as a spectroscopically pure oil, $[\alpha]_{\text{D}}^{25}$ ₅₄₆ –79°. The absolute configuration, which corresponds to retention of configuration at rhenium, was assigned by analogy to similar substitution reactions of optically active triflate complex $(+)(R)\text{-3}$.²⁰ Complex $(-)(S)\text{-2b}$ was treated with *t*-BuO⁻K⁺. Workup gave spectroscopically pure di(*p*-tolyl)phosphido complex $(+)(S)\text{-4b}$ (76%) as an air-sensitive powder, $[\alpha]_{\text{D}}^{25}$ ₅₄₆ 397°. The related optically active, configurationally stable diphenylphosphido complex $(+)(S)\text{-}(\eta^5\text{-C}_5\text{H}_4\text{PPh}_2)\text{Re}(\text{NO})(\text{PPh}_3)(\text{PPh}_2)$ has also been recently reported.²⁵

2. X-ray Crystal Structures of Phosphido Complexes. Suitable single crystals of diphenylphosphido complex **4a** were obtained from benzene/hexane, and X-ray data were collected under the conditions summarized in Table II. Refinement, described in the Experimental Section, yielded the structure shown in Figure 2. Positional parameters, bond distances, and bond angles are summarized in Tables III–V. Since thermal parameters and structure factors were reported in the supplementary material of our preliminary communication,^{19a} and elsewhere,²⁶ they are not republished here.

As shown in Figure 2, the phosphido phosphorus atom (P2) is distinctly pyramidal. The sum of the three bond angles about P2 (103.8°, 107.5°, 111.7°) is 323.0°. This sum would be 328.5° for an idealized tetrahedral atom or 360.0° for a planar atom.

The Re–PPh₃ bond lies in the plane of the rhenium-fragment HOMO shown in Ib. The torsion angle between the PPh₂ lone pair and the Re–PPh₃ bond is thus a measure of the “gauche

(17) Bodner, G. S.; Patton, A. T.; Smith, D. E.; Georgiou, S.; Tam, W.; Wong, W.-K.; Strouse, C. E.; Gladysz, J. A. *Organometallics* **1987**, *6*, 1954.

(18) (a) Buhro, W. E.; Georgiou, S.; Fernández, J. M.; Patton, A. T.; Strouse, C. E.; Gladysz, J. A. *Organometallics* **1986**, *5*, 956. (b) Fernández, J. M.; Emerson, K.; Larsen, R. D.; Gladysz, J. A. *J. Am. Chem. Soc.* **1986**, *108*, 8268.

(19) (a) Buhro, W. E.; Georgiou, S.; Hutchinson, J. P.; Gladysz, J. A. *J. Am. Chem. Soc.* **1985**, *107*, 3346. (b) Buhro, W. E.; Gladysz, J. A. *Inorg. Chem.* **1985**, *24*, 3505.

(20) Merrifield, J. H.; Fernández, J. M.; Buhro, W. E.; Gladysz, J. A. *Inorg. Chem.* **1984**, *23*, 4022.

(21) Abbreviations: (a) OTs = OSO₂(*p*-Tol). (b) *p*-Tol = *p*-C₆H₄CH₃. (c) OTf = OSO₂CF₃.

(22) Kraihanzel, C. S. *J. Organomet. Chem.* **1974**, *73*, 137.

(23) (a) Gorenstein, D. L. *Phosphorus-31 NMR*; Academic: New York, 1984; pp 14–15. (b) Pregoson, P. S.; Kunz, R. W. ³¹P and ¹³C NMR of Transition Metal Phosphine Complexes; Springer-Verlag: New York, 1979; p 48.

(24) Absolute configurations are assigned according to the Baird/Sloan modification of the Cahn–Ingold–Prelog priority rules. The $\eta^5\text{-C}_5\text{H}_5$ ligand is considered to be a pseudoatom of atomic number 30, which gives the following sequence: $\eta^5\text{-C}_5\text{H}_5 > \text{PAR}_3 > \text{PAR}_2\text{H} > \text{PAR}_2 > \text{OTs} > \text{NO}$. In complexes with more than one chiral center, the rhenium configuration is specified first. Stanley, K.; Baird, M. C. *J. Am. Chem. Soc.* **1975**, *97*, 6598. Sloan, T. E. *Top. Stereochem.* **1981**, *12*, 1.

(25) Zwick, B. D.; Arif, A. M.; Patton, A. T.; Gladysz, J. A. *Angew. Chem., Int. Ed. Engl.* **1987**, *26*, 910.

(26) Buhro, W. E. Ph.D. Thesis, UCLA, 1985.

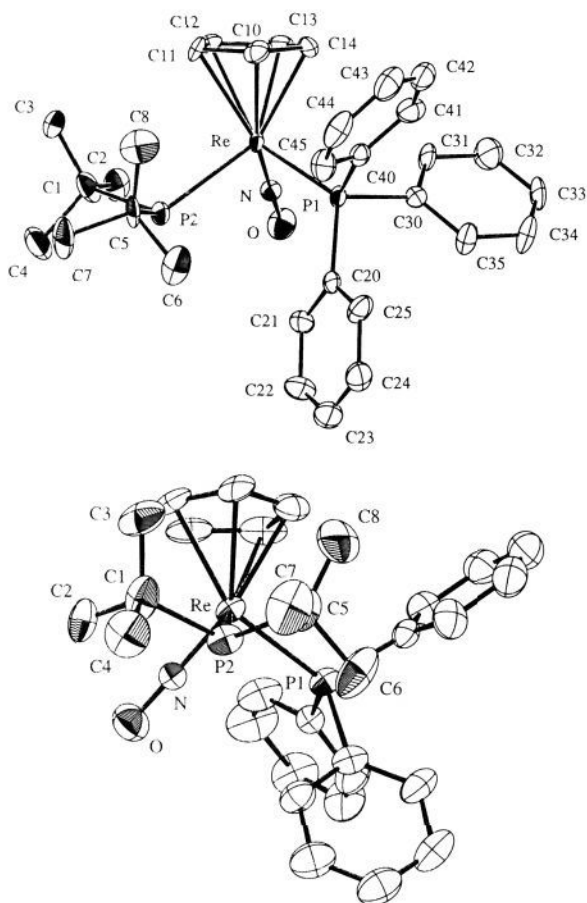


Figure 3. Two views of the molecular structure of $(\eta^5\text{-C}_5\text{H}_5)\text{Re}(\text{NO})(\text{PPh}_3)(\text{P}(t\text{-Bu})_2)$ (**4d**).

effect" and is calculated to be 59.7° (Experimental Section). The Re-PPh₂ bond (2.461 (3) Å) is significantly longer than the Re-PPh₃ bond (2.358 (3) Å).

Suitable single crystals of **4d** were obtained from ether/heptane, and X-ray data were collected under the conditions summarized in Table II. Refinement, described in the Experimental Section, yielded the structure shown in Figure 3. Positional parameters, bond distances, and bond angles are summarized in Tables VI-VIII.

The sum of the three bond angles about the phosphido phosphorus atom (P2) in **4d** (108.7° , 108.7° , 114.7°) is 332.1° . Thus, P2 is less pyramidal than in **4a**. The torsion angle between the PR₂ lone pair and the Re-PPh₃ bond is 58.9° . The Re-PR₂ bond (2.526 (4) Å) is longer than that in **4a**, and the P1-Re-P2 angle ($100.0 (1)^\circ$) is the largest deviation from the 90° L-Re-L' angles in idealized octahedral structure II observed to date.

3. MO Calculations. The structures of **4a-d** were further analyzed by extended-Hückel MO (EHMO) calculations on the model compound $(\eta^5\text{-C}_5\text{H}_5)\text{Re}(\text{NO})(\text{PH}_3)(\text{PH}_2)$, as described in the Experimental Section. The PH₂ phosphorus was assigned a tetrahedral geometry, and the Re-PH₂ bond length was taken from the crystal structure of **4a**. The PH₂ fragment lone pair was found to be 1.7905 eV lower in energy than the HOMO of the $[(\eta^5\text{-C}_5\text{H}_5)\text{Re}(\text{NO})(\text{PH}_3)]^+$ fragment (shown in Ia).

Figure 4 (bottom) shows the variation in E_{total} as the PH₂ ligand was rotated. The curve exhibits two nondegenerate energy minima and two nondegenerate energy maxima. At the global minimum ($\theta = 320^\circ$), the PH₂ lone pair resides between the $\eta^5\text{-C}_5\text{H}_5$ and PH₃ ligands and makes a 95° torsion angle with the Re-PH₃ bond and rhenium-fragment HOMO. At the local minimum ($\theta = 150^\circ$), the PH₂ lone pair resides between the NO and PH₃ ligands and makes a 75° torsion angle with the Re-PH₃ bond. This corresponds well with the ca. 60° torsion angles found in the structures of **4a** and **4d** above. At the energy maxima in Figure

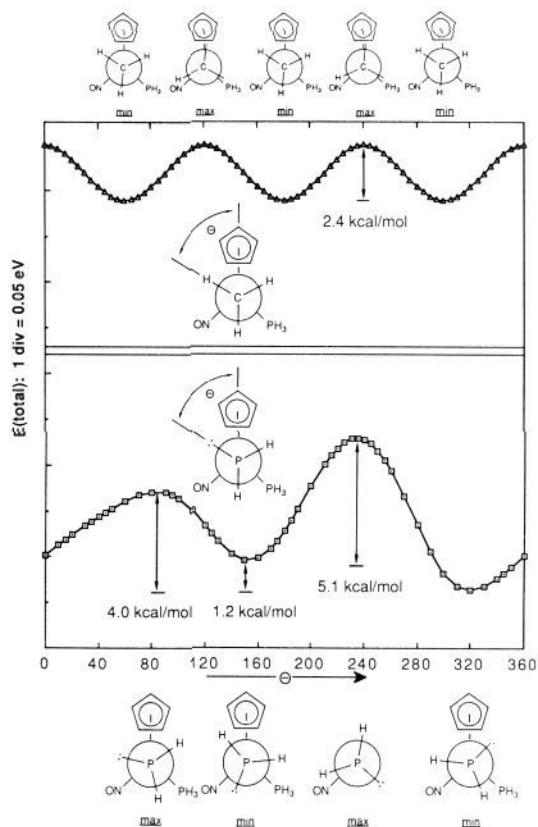


Figure 4. Bottom: Variation in E_{total} for phosphido complex $(\eta^5\text{-C}_5\text{H}_5)\text{Re}(\text{NO})(\text{PH}_3)(\text{PH}_2)$ as the PH₂ ligand is rotated, calculated by the extended-Hückel method with weighted H_{ij} formula. Top: Corresponding calculation for methyl complex $(\eta^5\text{-C}_5\text{H}_5)\text{Re}(\text{NO})(\text{PH}_3)(\text{CH}_3)$ as the CH₃ ligand is rotated; data from ref 16b.

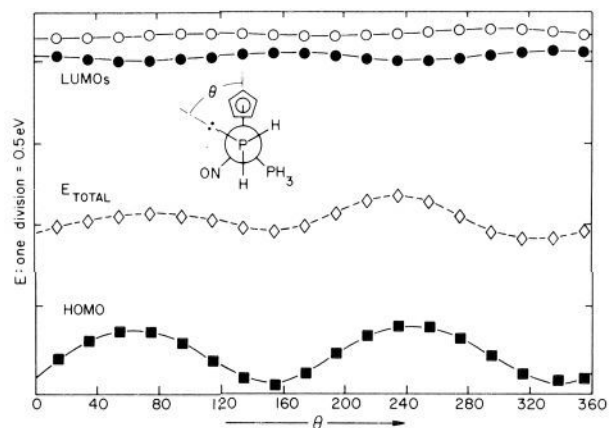


Figure 5. Variation in the HOMO and LUMO energies in $(\eta^5\text{-C}_5\text{H}_5)\text{Re}(\text{NO})(\text{PH}_3)(\text{PH}_2)$ as the PH₂ ligand is rotated. Calculated as in Figure 4 with the E_{total} included at an arbitrary energy value for comparison.

4 ($\theta = 235^\circ$, 80°), the PH₂ lone pair is syn (torsion angle 10°) and approximately anti (torsion angle 145°) to the Re-PH₃ bond. This E_{total}/θ curve markedly contrasts with that for CH₃ ligand rotation in model complex $(\eta^5\text{-C}_5\text{H}_5)\text{Re}(\text{NO})(\text{PH}_3)(\text{CH}_3)$, which is replotted from a previous paper in Figure 4 (top)^{16b} and discussed below.

Figure 5 shows the variation in the HOMO and two LUMO energies of $(\eta^5\text{-C}_5\text{H}_5)\text{Re}(\text{NO})(\text{PH}_3)(\text{PH}_2)$ as the PH₂ ligand is rotated. The E_{total} from Figure 4 is included at an arbitrary energy value for comparison. The phase and amplitude correlation between the θ dependence of the HOMO and E_{total} is striking. In contrast, the LUMO energies show no significant correlation with either E_{total} or the HOMO energy.

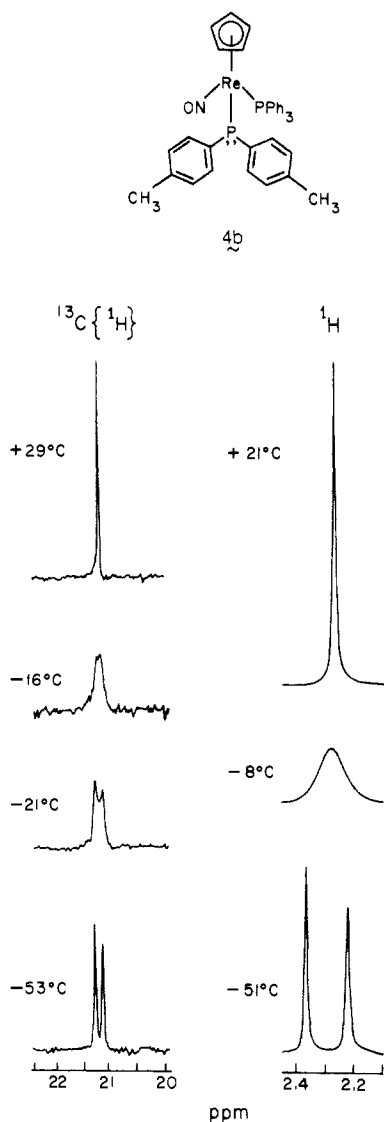


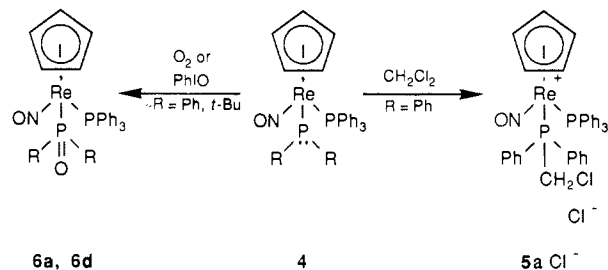
Figure 6. Methyl resonances in variable-temperature $^{13}\text{C}\{^1\text{H}\}$ and ^1H NMR spectra of $(\eta^5\text{-C}_5\text{H}_5)\text{Re}(\text{NO})(\text{PPh}_3)(\text{P}(p\text{-Tol})_2)$ (**4b**).

At the HOMO energy minima ($\theta = 155^\circ, 335^\circ$), the HOMO was found to be the rhenium-centered orbital Ia. At the energy maxima ($\theta = 55^\circ, 235^\circ$), the HOMO was found to be a combination of Ia and the PH_2 lone pair. The PH_2 phosphorus-atom charge contribution to the HOMO was found to follow the same θ dependence as the HOMO energy. At the minima, the PH_2 phosphorus accounted for only 0.02 electron of the two electrons in the HOMO. At the maxima, the PH_2 phosphorus contribution increased to 0.20 to 0.25 electron. At the minima and maxima, rhenium made by far the greatest contribution to the HOMO charge (1.39–1.45 electrons). Contributions to the HOMO charge by other atoms were very small.

4. Dynamic Behavior of Phosphido Complexes. The $^{31}\text{P}\{^1\text{H}\}$ NMR spectrum of di(*p*-tolyl)phosphido complex **4b** was essentially temperature independent over the range -62 to $+50^\circ\text{C}$. However, ^1H and $^{13}\text{C}\{^1\text{H}\}$ NMR spectra showed a dynamic process that exchanged the diastereotopic *p*-tolyl groups (Figure 6). As described in the Experimental Section, $\Delta G_{264\text{K}}^\ddagger = 13.0 \pm 0.1$ kcal/mol and $\Delta G_{255\text{K}}^\ddagger = 13.3 \pm 0.2$ kcal/mol were calculated from the coalescence of the ^1H and ^{13}C NMR methyl resonances, respectively.

Dynamic processes also exchanged the diastereotopic ethyl and *tert*-butyl groups in **4c** and **4d**. For **4c**, coalescence of the ^1H and ^{13}C NMR methyl resonances gave $\Delta G_{312\text{K}}^\ddagger = 14.9 \pm 0.1$ kcal/mol and $\Delta G_{308\text{K}}^\ddagger = 14.7 \pm 0.1$ kcal/mol. For **4d**, coalescence of the ^1H NMR methyl resonances gave $\Delta G_{266\text{K}}^\ddagger = 12.6 \pm 0.1$ kcal/mol. A dynamic process that exchanged the diastereotopic phenyl

Scheme II. Reactions of Rhenium Phosphido Complexes



groups in **4a** was evident from $^{13}\text{C}\{^1\text{H}\}$ NMR spectra (Table I). Quantitative data are summarized in Table IX.

Importantly, the couplings $^2J_{\text{PP}}$ in **4a–d** were retained in $^{31}\text{P}\{^1\text{H}\}$ NMR spectra recorded as high as $50\text{--}60^\circ\text{C}$. This bounds ΔG^\ddagger for phosphido ligand dissociation as >17 kcal/mol and excludes a dissociative mechanism for exchange of the diastereotopic aryl or alkyl groups. Note that simple Re-PR_2 bond rotation is incapable of exchanging the diastereotopic groups. Hence, the above data require an inversion of configuration, which could in principle occur either at rhenium or phosphorus. However, the successful synthesis of optically active **4b** (see above) indicates that any inversion at rhenium must occur with a barrier substantially greater than 15 kcal/mol. Hence, phosphorus inversion must occur with exceptionally low barriers in **4a–d**.

5. Reactions and Phosphido Complexes. We sought to probe the nucleophilicity of the phosphido phosphorus lone pair in **4**. In CH_2Cl_2 , diphenylphosphido complex **4a** was readily alkylated (25°C , ca. 0.5 h) to give bis(phosphine) complex $[(\eta^5\text{-C}_5\text{H}_5)\text{Re}(\text{NO})(\text{PPh}_3)(\text{PPh}_2\text{CH}_2\text{Cl})]^+\text{Cl}^-$ (**5a-Cl⁻**; Scheme II). Workup gave the crystalline solvate **5a-Cl⁻·CH₂Cl₂** in 79% yield. Complex **5a-Cl⁻·CH₂Cl₂** was characterized identically to the other new phosphine complexes (Table I), and the new methylene group was obvious in ^1H and ^{13}C NMR spectra.

Solutions of **4a** gave intractable product mixtures when exposed to air. However, addition of only a few equivalents of O_2 (as air) to **4a** (25°C , 21 h, THF) gave phosphine oxide $(\eta^5\text{-C}_5\text{H}_5)\text{Re}(\text{NO})(\text{PPh}_3)(\text{P}(\text{=O})\text{Ph}_2)$ (**6a**, Scheme II) in 45–70% yields. Complex **6a** was also prepared in 60% yield from **4a** and iodobenzene, PhIO. Reaction of di(*tert*-butyl)phosphido complex **4d** with iodobenzene gave phosphine oxide $(\eta^5\text{-C}_5\text{H}_5)\text{Re}(\text{NO})(\text{PPh}_3)(\text{P}(\text{=O})(t\text{-Bu})_2)$ (**6d**) in 34% yield after recrystallization. Complexes **6a** and **6d** were characterized identically to **4a–d** and exhibited $\text{P}=\text{O}$ $^{31}\text{P}\{^1\text{H}\}$ NMR resonances (Table I) close to those of $\text{Ph}_3\text{P}=\text{O}$ (27.0 ppm) and $\text{Me}_3\text{P}=\text{O}$ (36.2 ppm).²⁷ The KBr IR spectrum of **6a** showed unique, medium-intensity absorptions at 1113, 1087, 1075, and 1061 cm^{-1} .

Discussion

1. Geometry at Phosphorus. Although we have emphasized the pyramidal nature of the phosphido phosphorus atom in complexes **4a** and **4d**, the bond angles about phosphorus ($104\text{--}115^\circ$) are larger than typically found in simple organophosphines such as PMe_3 (99°) and PPh_3 (103°).²⁸ Other X-ray crystal structures of pyramidal terminal phosphido complexes have been reported,¹³ and this trend appears general. For example, Weber^{13c} and Paine^{13c} found average bond angles of 106° and 105° about the Fe-PX_2 phosphorus atoms in $(\eta^5\text{-C}_5\text{Me}_5)\text{Fe}(\text{CO})_2(\text{PPh}_2)$ and $(\eta^5\text{-C}_5\text{Me}_5)\text{Fe}(\text{CO})_2(\text{PN}(\text{CH}_3)\text{CH}_2\text{CH}_2\text{NCH}_3)$ (see IV). Roper could not locate the Os-PPhH hydrogen in $\text{Os}(\text{CO})_2(\text{PPh}_3)_2\text{-Cl}(\text{PPhH})$ but did determine an Os-P-C angle of 113° .^{13b}

The large bond angles about the pyramidal phosphido phosphorus in **4a**, **4d**, and other complexes are probably due to steric and electronic effects of the bulky, electron-releasing transition-

(27) (a) Moedritzer, K.; Maier, L.; Groenweghe, L. C. D. *J. Chem. Eng. Data* 1962, 7, 307. (b) Crutchfield, M. M.; Dungan, C. H.; Letcher, J. H.; Mark, V.; Van Wazer, J. R. In *Topics in Phosphorus Chemistry*; Grayson, M., Griffith, E. J., Eds.; Wiley-Interscience: New York, 1967; Vol. 5.

(28) Corbridge, D. E. C. *The Structural Chemistry of Phosphorus*; Elsevier: New York, 1974; Tables 50 and 51.

Table I. Spectroscopic Characterization of New Rhenium Phosphine and Phosphido Complexes

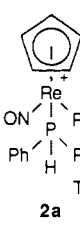
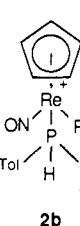
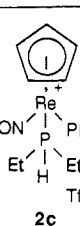
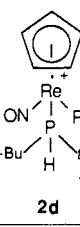
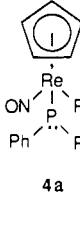
Complex	IR (cm^{-1} , KBr)	^1H NMR (δ) ^a	$^{31}\text{P}\{^1\text{H}\}$ NMR (ppm) ^b	$^{13}\text{C}\{^1\text{H}\}$ NMR (ppm) ^c
	3150-2840 m, $\nu_{\text{P-H}}$ 2292 m, $\nu_{\text{N=O}}$ 1727 vs. 1585 w, 1574 w, 1495 w, 1481 m, 1436 s, 1416 m, 1387 w, 1313 w, 1283 w, 1276 w, 1216-1182 s vbr, 1161 m, 1118 m, 1094 m, 1076 m, 1032 m, 1011 s, 998 m, 937 m, 916 m, 884 m, 857 m, 820 m, 747 s, 696 s, 678 s.	7.72 (d, $J_{\text{HH}} = 7.9$ Hz, 2H), 7.56-7.09 (m, 27H), 7.52 (dd, $^1J_{\text{HP}} = 397$ Hz, $^3J_{\text{HP}} = 4.9$ Hz, 1H), 5.38 (s, 5H), 2.32 (s, 3H). ^d	12.38 (d, $J_{\text{pp}} = 13.0$ Hz, PPh_3), -7.54 (d, $J_{\text{pp}} = 13.0$ Hz, PPH_2H). ^{d,e}	OTs at 145.37 (s, \downarrow), 138.60 (s, \uparrow), 128.59 (s, m), 126.68 (s, p), 21.33 (s, CH_3); PPh_3 at 133.52 (d, $J = 11.0$ Hz, \uparrow), 132.43 (d, $J = 57.6$ Hz, \downarrow), 131.93 (br s, p), 129.62 (d, $J = 10.9$ Hz, m); PPh_2H at 133.25 (d, $J = 11.0$ Hz, \uparrow), 132.07 (d, $J = 10.1$ Hz, \uparrow), 131.66 (br s, p), 129.89 (d, $J = 11.9$ Hz, m), 129.74 (d, $J = 11.6$ Hz, m); ^f 93.09 (s, C_5H_5). ^g
	3109 w, 3062 m, 2920 w, $\nu_{\text{P-H}}$ 2294 w, $\nu_{\text{N=O}}$ 1716 vs, 1598 m, 1498 m, 1481 m, 1435 m, 1423 m, 1398 m, 1313 w, 1273 w, 1221 s, 1208 s, 1190 s, 1163 m, 1119 m, 1096 m, 1034 m, 1013 m, 998 m, 917 m, 894 m, 870 w, 848 w, 811 m, 753 m, 726 m, 697 s, 678 s, 634 m, 622 m.	7.75 - 7.03 (m, 27H), 7.40 (dd, $^1J_{\text{HP}} = 394.7$ Hz, $^3J_{\text{HP}} = 5.1$ Hz, 1H), 5.36 (s, 5H), 2.37 (s, 6H), 2.31 (s, 3H). ^d	13.07 (d, $J_{\text{pp}} = 13.2$ Hz, PPh_3), -8.86 (d, $J_{\text{pp}} = 13.4$ Hz, PAR_2H) ($^1J_{\text{PH}} = 396$ Hz). ^{d,h}	OTs at 146.50 (s, \downarrow), 139.01 (s, \uparrow), 128.97 (s, m), 126.77 (s, p), 21.41 (s, CH_3); PPh_3 at 133.96 (d, $J = 11.0$ Hz, \uparrow), 132.86 (d, $J = 57.7$ Hz, \downarrow), 132.39 (d, $J = 2.6$ Hz, p), 130.03 (d, $J = 11.0$ Hz, m) PAR_2H at 143.23 (br s, p), 142.97 (d, $J = 2.5$ Hz, p), 133.96 (d, $J = 11.0$ Hz, \uparrow), 132.00 (d, $J = 10.2$ Hz, \uparrow), 131.00 (d, $J = 11.1$ Hz, m), 130.92 (d, $J = 11.9$ Hz, m), 129.03 (d, $J = 59.6$ Hz, \downarrow), 126.66 (d, $J = 59.7$ Hz, \downarrow), 21.57 (s, 2CH_3); ^d 93.38 (s, C_5H_5). ^d
	3079 m, 2968 w, 2936 w, 2877 w, $\nu_{\text{P-H}}$ 2326 w, $\nu_{\text{N=O}}$ 1699 vs, 1586 w, 1573 w, 1482 m, 1458 w, 1436 s, 1422 m, 1384 w, 1359 w, $\nu_{\text{C-F}}$ 1267 vs, 1224 s, 1185 m, 1153 s, 1095 m, 1030 vs, 998 m, 887 m, 854 m, 749 m, 696 s, 637 vs.	7.55-7.52 (m, 9H), 7.31-7.24 (m, 6H), 5.54 (s, 5H), 5.19 (br d, $^1J_{\text{HP}} =$ 368.9 Hz, 1H), 2.17-2.04 (m, 1H), 1.97-1.83 (m, 3H), 1.17-1.02 (m, 6H). ⁹	14.66 (d, $J_{\text{pp}} = 14.9$ Hz, PPh_3), -17.72 (d, $J_{\text{pp}} = 14.9$ Hz, PR_2H). ^{g,j}	PPh_3 at 133.02 (d, $J = 10.8$ Hz, \uparrow), 132.45 (dd, $^1J = 56.5$ Hz, $^3J = 1.3$ Hz, \downarrow), 131.70 (d, $J =$ 2.6 Hz, p), 129.36 (d, $J = 10.8$ Hz, m); 91.83 (s, C_5H_5), 18.63 (dd, $^1J = 34.9$ Hz, $^2J = 0.8$ Hz, PCl_2), 16.84 (dd, $^1J = 37.8$ Hz, $^3J = 1.1$ Hz, PCl_2), 12.06 (d, $J = 7.3$ Hz, CH_3), 9.81 (d, $J =$ 3.8 Hz, C^*H_3). ^{g,k}
	3360 w, 3063 m, 3029 m, 2962 m, $\nu_{\text{P-H}}$ 2319 m, $\nu_{\text{N=O}}$ 1692 vs, 1575 m, 1482 s, 1457 m, 1435 s, 1374 s, $\nu_{\text{C-F}}$ 1267 vs, 1225 s, 1145 vs, 1091 s, 1032 vs, 1000 s, 943 m, 866 s, 756 s, 695 s.	7.55-7.52 (m, 9H), 7.27-7.22 (m, 6H), 5.69 (s, 5H), 5.35 (dd, $^1J_{\text{HP}} = 358.4$ Hz, $^3J_{\text{HP}} = 4.0$ Hz, 1H), 1.29 (d, $^3J_{\text{HP}} = 15.2$ Hz, 9H), 1.08 (d, $^3J_{\text{HP}} = 15.2$ Hz, 9H). ^d	40.15 (d, $J_{\text{pp}} = 10.0$ Hz, PR_2H), 6.89 (d, $J_{\text{pp}} = 10.0$ Hz, PPh_3). ^g	PPh_3 at 133.66 (d, $J = 10.2$ Hz, \uparrow), 132.03 (s, p), 129.62 (d, $J = 10.0$ Hz, m); 91.44 (s, C_5H_5), 40.02 (d, $J =$ 28.4 Hz, PCl_2), 35.80 (d, $J = 22.8$ Hz, PCl_2), 32.35 (d, $J = 3.7$ Hz, 3CH_3), 31.33 (d, $J = 2.9$ Hz, $3\text{C}^*\text{H}_3$). ^{d,k}
	3302 w, 3057 m, 3042 m, $\nu_{\text{N=O}}$ 1664 vs, 1578 m, 1480 m, 1475 m, 1435 w, 1425 m, 1307 w, 1187 w, 1100 m, 1090 w, 1025 w, 1000 m, 993 m, 838 m, 831 m, 818 m, 811 m, 751 m, 744 s, 735 m, 700 s, 695 s.	7.55-6.89 (m, 25H), 4.91 (s, 5H). ^l	19.45 (d, $J_{\text{pp}} = 15$ Hz, PPh_3), -48.29 (d, $J_{\text{pp}} =$ 15 Hz, PPH_2). ^{h,l}	PPh_2 at 134.88 (br d, $J = 20.1$ Hz, \uparrow), 128.29 (d, $J = 5.5$ Hz, m), 126.07 (s, p); ^f PPh_3 at 137.08 (d, $J = 52.3$ Hz, \downarrow), 135.39 (dd, $^2J = 10.6$ Hz, $^4J = 2.2$ Hz, \uparrow), 131.07 (d, $J =$ 2.5 Hz, p), 129.10 (d, $J = 10.3$ Hz, m); 92.39 (s, C_5H_5). ^{l,1} PPh_2 at 157.48 (d, $J = 33.8$ Hz, \downarrow), 147.72 (d, $J = 25.2$ Hz, \downarrow), 137.20 (br d, $J = 21.1$ Hz, \downarrow), 131.56 (br d, $J = 16.5$ Hz, \uparrow), 128.89 (br s, m), 128.16 (br s, p), 127.91 (br s, m), 123.89 (br s, p); PPh_3 at 136.32 (d, $J = 52.3$ Hz, \downarrow), 135.58 (d, $J = 9.2$ Hz, \uparrow), 131.18 (s, p), 129.13 (d, $J =$ 10.1 Hz, m); 92.40 (s, C_5H_5). ^{l,m}

Table I (Continued)

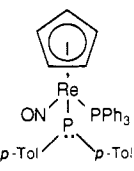
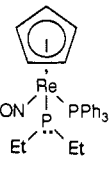
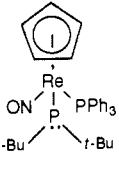
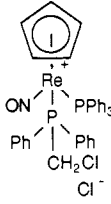
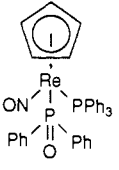
Complex	IR (cm ⁻¹ , $\nu_{N\equiv O}$)	¹ H NMR (δ) ^a	³¹ P{ ¹ H} NMR (ppm) ^b	¹³ C{ ¹ H} NMR (ppm) ^c
 <p>4b</p>	3092-2661 w, $\nu_{N\equiv O}$ 1649 vs, 1571 w, 1491 m, 1481 m, 1434 m, 1265 w, 1183 w, 1106 m, 1094 m, 1000 w, 844 w, 805 m, 756 w, 747 m, 695 m.	7.97-6.83 (m, 23H), 4.87 (s, 5H), 2.28 (s, 6H). ¹ ----- 7.42-6.48 (m, 23H), 4.91 (s, 5H), 2.37 (s, 3H), 2.23 (s, 3H). ^{1,e}	19.23 (d, $J_{PP} =$ 15.3 Hz, PPh ₃), -50.98 (d, $J_{PP} =$ 15.3 Hz, PAR ₂). ^{h,1}	PPh ₃ at 137.14 (d, $J = 53.1$ Hz, 1J), 135.38 (dd, $^2J = 10.5$ Hz, $^4J = 2.2$ Hz, ϕ). ⁿ 130.96 (d, $J = 1.8$ Hz, ρ), 128.99 (d, $J = 10.2$ Hz, m); PAR ₂ at 149.5 (v br, $\underline{1}$), 134.82 br d, $J = 18.3$ Hz, ϕ). ⁿ 129.03 (d, $J = 4.6$ Hz, m), 21.17 (s, 2CH ₃); 92.34 (s, C ₅ H ₅). ^{1,1} ----- PPh ₃ at 136.36 (d, $J = 52.3$ Hz, $\underline{1}$), 135.28 (d, $J = 10.1$ Hz, ϕ), 131.10 (s, ρ), 129.03 (d, $J =$ 10.8 Hz, m); PAR ₂ at 153.79 (d, $J = 33.0$ Hz, $\underline{1}$), 144.33 (d, $J = 27.5$ Hz, $\underline{1}$), 137.70 (s, ρ), 137.10 (d, $J =$ 22.0 Hz, ϕ), 132.75 (s, ρ), 131.58 (d, $J = 15.6$ Hz, ϕ), 129.49 (d, $J = 7.3$ Hz, m), 128.66 (s, m), 21.34 (br s, CH ₃), 21.21 (br s, ¹ H ₃); 92.33 (s, C ₅ H ₅). ^{1,0}
	 <p>4c</p>	3243 w, 3013 m, 2946 m, 2913 m, 2861 m, 2811 w, 2234 w, $\nu_{N\equiv O}$ 1635 vs, 1586 m, 1573 m, 1481 m, 1451 m, 1436 s, 1419 m, 1189 w, 1092 s, 998 m, 811 m, 751 s, 702 s, 693 s, 656 w.	7.64-7.60 (m, 6H), 7.58-6.98 (m, 9H), 4.68 (s, 5H), 1.48 (m, $J = 7$ Hz, 4H), 1.19 (m, $J = 7$ Hz, 6H). ⁹ ----- 7.68-7.62 (m, 6H), 7.09-6.97 (m, 9H), 4.62 (s, 5H), 2.21 (br, 1H), 1.52 (br, 3H), 1.40 (br, 3H), 1.23 (br, 3H). ^p	18.87 (d, $J_{PP} = 14.6$ Hz, PPh ₃), -45.69 (d, $J_{PP} = 14.6$ Hz, PR ₂). ^{k,p}
 <p>4d</p>		3060 w, 2784 m, 2844 m, $\nu_{N\equiv O}$ 1656 vs, 1571 w, 1477 m, 1433 s, 1377 m, 1163 m, 1092 m, 1081 m, 1000 m, 814 m, 744 m, 692 s.	7.51-7.43 (m, 6H), 7.37-7.29 (m, 9H), 5.27 (s, 5H), 1.09 (d, $^3J_{HP} = 9.4$ Hz, 18H). ¹ ----- 7.49-7.34 (br s, 15H), 5.32 (s, 5H), 1.28 (d, $^3J_{HP} = 9.2$ Hz, 9H), 0.86 (d, $^3J_{HP} = 10.1$ Hz, 9H). ^{1,r}	19.70 (d, $J_{PP} = 13.0$ Hz, PPh ₃), 8.58 (d, $J_{PP} = 13.0$ Hz, PR ₂). ¹
	 <p>5a</p>	3110-2800 m, $\nu_{N\equiv O}$ 1696 vs, 1584 w, 1572 w, 1479 m, 1433 s, 1422 m, 1393 w, 1310 w, 1278 w, 1182 w, 1140 w, 1093 s, 1072 m, 1025 w, 997 m, 885 w, 857 w, 828 m, 802 m, 747 s, 731 s, 696 s, 659 m.	7.76-7.26 (m, 20H), 7.06-6.94 (m, 5H), 5.55 (s, 5H), 5.36 (s, CH ₂ Cl ₂ solvate), 4.06 (d, $J_{HH} = 13.6$ Hz, 1H), 3.94 (dd, $J_{HH} = 13.6$ Hz, $^2J_{HP} = 2.1$ Hz, 1H). ^d	8.87 (d, $J_{PP} =$ 8.4 Hz, PPh ₃), 6.54 (d, $J_{PP} =$ 8.4 Hz, PPh ₂ CH ₂ Cl). ^{d,m}
 <p>6a</p>		3060 m, 3000 m, 2985 m, $\nu_{N\equiv O}$ 1679 vs, 1586 w, 1574 w, 1493 w, 1478 m, 1434 s, 1356 w, 1332 w, 1304 w, 1274 w, 1202 w, 1182 w, 1166 w, 1113 m, ^t 1097 m, 1087 m, ^t 1075 m, ^t 1061 m, ^t 1027 m, 998 m, 967 w, 916 m, 858 w, 845 w, 819 m, 756 m, 749 m, 743 m, 736 m, 721 w, 700 s, 690 s, 620 w.	7.79-7.71 (m, 3H), 7.49-7.17 (m, 19H), 7.03-6.89 (m, 3H), 4.99 (s, 5H). ^d	36.36 (d, $J_{PP} =$ 153.50 Hz, PPh ₂ O), 14.76 (d, $J_{PP} =$ 20.1 Hz, PPh ₃). ^{d,m}

Table I (Continued)

Complex	IR (cm^{-1} , KBr)	^1H NMR (τ) ^a	^{31}P (^1H) NMR (ppm) ^d	^{13}C (^1H) NMR (ppm) ^c
 6d	3002 m, 2984 m, 2962 m,	7.61-7.55 (m, 6H),	86.86 (br d, $J_{\text{PP}} = 17.1$ Hz,	PPh ₃ at
	2891 m, 2860 m, $\nu_{\text{N=O}}$	7.36-7.34 (m, 9H),	PR ₂ O,	137.08 (d, $J = 52.7$ Hz, ρ),
	1663 vs, 1587 w, 1574 w,	5.29 (s, 5H),	9.66 (br d, $J_{\text{PP}} = 17.1$ Hz,	134.54 (d, $J = 10.2$ Hz, ρ),
	1481 m, 1434 s, 1380 m,	1.19 (d, $^3J_{\text{HP}} = 12.6$ Hz, 9H),	PPh ₃) ^d ,	130.28 (s, ρ),
	1358 m, 1184 m, 1069 s,	0.76 (d, $^3J_{\text{HP}} = 12.4$ Hz, 9H) ^d ,		128.31 (d, $J = 10.2$ Hz, ρ);
	1014 m, 834 m, 817 m,			91.41 (s, C ₅ H ₅),
	805 m, 743 s, 696 s,			45.68 (d, $J = 27.0$ Hz, PC),
	604 m,			42.95 (d, $J = 23.5$ Hz, PC ¹),
				29.77 (d, $J = 3.9$ Hz, 3C _{CH₃}),
				28.87 (d, $J = 4.0$ Hz, 3C _{H₃}) ^d ,

^a At 300 MHz and ambient probe temperature and referenced to internal Si(CH₃)₄ except where noted. ^b At 32 MHz and ambient probe temperature and referenced to external 85% H₃PO₄ except where noted. ^c At 75 MHz and ambient probe temperature and referenced to internal Si(CH₃)₄ except where noted. All couplings are to phosphorus unless noted. Assignments of resonances to the PPh₃ carbons were made as described in footnote c of Table I in ref 18a. ^d In CD₂Cl₂. ^e At -51 °C. ^f Ipso carbon not observed. ^g In CDCl₃. ^h At -30 °C. ⁱ In THF-d₈. ^j CF₃ carbon not observed. ^k At 121 MHz. ^l At 63 °C. ^m At -25 °C. ⁿ These resonances obscure the para carbon. ^o At -21 °C. ^p In C₆D₆. ^q In toluene-d₈ at 65 °C. ^r At -73 °C. ^s One or both para carbons not observed. ^t These absorptions are likely derived from the P=O functionality.

metal substituents. As a result, the phosphorus lone pair should have increased p character. Accordingly, **4a-d** and other terminal phosphido complexes (see below) are highly nucleophilic. This property is likely responsible for the ease of formation of bridging phosphido complexes from terminal phosphido complexes.^{25,29}

The metal-phosphido phosphorus bond in Os(CO)₂(PPh₃)₂(Cl)(PPhH) (2.523 (7) Å) is longer than the metal-phosphine phosphorus bond (2.414 (6) Å), analogous to **4a** and **4d**. One of the major factors that likely contribute to this bond lengthening—nonbonding electron-pair repulsion¹⁰ between the transition metal and phosphido ligand—is analyzed in the following section.

2. Conformational Analysis: The "Gauche Effect". We first sought theoretical evidence for our hypothesis that a "gauche effect" should be an important conformation-determining factor in coordinatively saturated phosphido complexes. However, it is instructive to initially review an earlier EHMO calculation on the model methyl complex ($\eta^5\text{-C}_5\text{H}_5$)Re(NO)(PH₃)(CH₃) (Figure 4, top).^{16b} Here, three degenerate minima, with $\theta = 55\text{--}60^\circ$, $175\text{--}180^\circ$, and $295\text{--}300^\circ$, were found as the Re-CH₃ bond was rotated through 360° . These were separated by maxima that were 2.4 kcal/mol higher in energy. Note that these complexes are octahedral, and hence the bond angles about rhenium (see II and III) do not permit perfectly staggered or eclipsed Re-CH₃ or Re-PH₂ conformations.

In contrast to the results with methyl complex ($\eta^5\text{-C}_5\text{H}_5$)Re(NO)(PH₃)(CH₃), only two minima are found as the Re-PH₂ bond is rotated through 360° in phosphido complex ($\eta^5\text{-C}_5\text{H}_5$)Re(NO)(PH₃)(PH₂) (Figure 4, bottom). Furthermore, the magnitudes of the barriers are greater than with ($\eta^5\text{-C}_5\text{H}_5$)Re(NO)(PH₃)(CH₃). Hence, there must be an important additional factor contributing to the Re-PH₂ conformational energy profile of ($\eta^5\text{-C}_5\text{H}_5$)Re(NO)(PH₃)(PH₂).

(29) The literature on bridging phosphido complexes is extensive; selected references: (a) Carty, A. J. *Adv. Chem. Ser.* **1982**, No. 196, 163. (b) Burckett-St. Laurent, J. C. T. R.; Haines, R. J.; Nolte, C. R.; Steen, N. D. C. T. *Inorg. Chem.* **1980**, *19*, 578. (c) Ritchey, J. M.; Zozulin, A. J.; Wroblewski, D. A.; Ryan, R. R.; Wasserman, H. J.; Moody, D. C.; Paine, R. T. *J. Am. Chem. Soc.* **1985**, *107*, 501. (d) Lang, H.; Zsolnai, L.; Huttner, G. J. *Organomet. Chem.* **1985**, *282*, 23. (e) Powell, J.; Sawyer, J. F.; Stainer, M. V. *J. Chem. Soc., Chem. Commun.* **1985**, 1314. (f) Regragui, R.; Dixneuf, P. H.; Taylor, N. J.; Carty, A. J. *Organometallics* **1986**, *5*, 1. (g) Baker, R. T.; Tulip, T. H. *Ibid.* **1986**, *5*, 839. (h) Kyba, E. P.; Davis, R. E.; Clubb, C. N.; Liu, S.-T.; Palacios, H. O. A.; McKennis, J. S. *Ibid.* **1986**, *5*, 869. (i) Rosenberg, S.; Mahoney, W. S.; Hayes, J. M.; Geoffroy, G. L.; Rheingold, A. L. *Ibid.* **1986**, *5*, 1065. (j) Rosenberg, S.; Lockledge, S. P.; Geoffroy, G. L. *Ibid.* **1986**, *5*, 2517. (k) Drew, M. G. B.; Wade, S. R.; Wallbridge, G. H.; Willey, G. R. *J. Chem. Soc., Dalton Trans.* **1986**, 713. (l) Gelmini, L.; Stephan, D. W. *Inorg. Chem.* **1986**, *25*, 1222. (m) King, R. B.; Fu, W.-K.; Holt, E. M. *Ibid.* **1986**, *25*, 2394. (n) Arif, A. M.; Jones, R. A.; Schwab, S. T.; Whittlesey, B. R. *J. Am. Chem. Soc.* **1986**, *108*, 1703. (o) Collum, D. B.; Klang, J. A.; Depue, R. T. *Ibid.* **1986**, *108*, 2333. (p) Shyu, S.-G.; Calliagaris, M.; Nardin, G.; Wojcicki, A. *Ibid.* **1987**, *109*, 3617. (q) Buhro, W. E.; Chisholm, M. H.; Folting, K.; Eichhorn, B. W.; Huffman, J. C. *J. Chem. Soc., Chem. Commun.* **1987**, 845. (r) Bullock, R. M.; Casey, C. P. *Acc. Chem. Res.* **1987**, *20*, 167.

Table II. Summary of Crystallographic Data for ($\eta^5\text{-C}_5\text{H}_5$)Re(NO)(PPh₃)(PH₂) (**4a**) and ($\eta^5\text{-C}_5\text{H}_5$)Re(NO)(PPh₃)(P(*t*-Bu)₂) (**4d**)

	4a	4d
molecular formula	C ₃₅ H ₃₀ NOP ₂ Re	C ₃₁ H ₃₈ NOP ₂ Re
formula weight	728.8	688.8
crystal system	monoclinic	triclinic
space group	P2 ₁ /a ^a	P1
cell dimensions		
<i>a</i> , Å	23.864 (6)	10.323 (3)
<i>b</i> , Å	10.233 (2)	11.892 (3)
<i>c</i> , Å	13.572 (3)	13.048 (3)
α , deg		85.72 (2)
β , deg	95.66 (2)	85.53 (2)
γ , deg		64.57 (2)
<i>V</i> , Å ³	3298 (1)	1440.8 (5)
<i>Z</i>	4	2
temp of collection	21 (1) °C	21 (1) °C
<i>d</i> _{calcd} , g/cm ³	1.47	1.59
<i>d</i> _{obsd} , g/cm ³ (22 °C)		1.58
crystal dimensions, mm	0.18 × 0.40 × 0.40	0.15 × 0.26 × 0.28
radiation, Å	λ (Mo K α) 0.71073	λ (Mo K α) 0.71073
data collection method	θ - 2θ	θ - 2θ
scan speed, deg/min ⁻¹	2.0-24.0 (variable)	2.4
reflections measd	+ <i>h</i> ,+ <i>k</i> ,± <i>l</i> ; 3.0-40°	+ <i>h</i> ,+ <i>k</i> ,± <i>l</i> ; 3.5-50°
scan range	K _{α1} - 1.0 to K _{α2} + 1.0	K _{α1} - 1.0 to K _{α2} + 1.0
no. of reflections between std	97	95
total unique data	3063	4350
cutoff for obsd data	<i>I</i> > 2.5(<i>I</i>)	<i>I</i> > 2.5 σ (<i>I</i>)
obsd data	2653	3080
abs coeff (μ), cm ⁻¹	38.2	44.0
method of refinement	block matrix least squares	block matrix least squares
no. of variables	361	314
$R = \sum(F_o - F_c) / \sum F_o $	0.055	0.057
$R_w = \sum(F_o - F_c)w^{1/2} / \sum F_o w^{1/2}$	0.062	0.064
weighting factor, <i>w</i>	1/($\sigma^2(F_o) + 0.0015(F_o)^2$)	1/ $\sigma^2(F_o)$
$\Delta\rho(\text{max})$, e Å ⁻³	2.51	5.26, 1.05 Å from Re

^a Nonstandard setting of P2₁/c [C_{2h}; No. 14] having equivalent positions $\pm(x,y,z)$ and $\pm(1/2-x, 1/2+y, z)$.

How do the three degenerate Re-CH₃ conformational minima of methyl complex ($\eta^5\text{-C}_5\text{H}_5$)Re(NO)(PH₃)(CH₃) manifest themselves in the bottom portion of Figure 4? The two Re-PH₂ minima ($\theta = 150^\circ$, 320°) can be derived by rotating the Re-CH₃ bonds in the $175\text{--}180^\circ$ and $295\text{--}300^\circ$ Re-CH₃ minima slightly clockwise and counterclockwise, respectively. This diminishes overlap of the rhenium-fragment HOMO and PH₂ lone pair. However, rhenium-fragment HOMO/PH₂ lone-pair overlap is at a maximum at $\theta = 60^\circ$ (and 240°), and this gives a local energy maximum in the vicinity of the third Re-CH₃ minimum at $55\text{--}60^\circ$. The global Re-PH₂ maximum ($\theta = 235^\circ$) enforces high rheni-

Table III. Atomic Coordinates of Non-Hydrogen Atoms in $(\eta^5\text{-C}_5\text{H}_5)\text{Re}(\text{NO})(\text{PPh}_3)(\text{PH}_2)$ (**4a**)

atom	x	y	z	$U(\text{eq}/\text{iso}) \times 10^4$
Re	0.25237 (2)	0.58146 (5)	0.69188 (3)	298
N	0.2222 (4)	0.4867 (10)	0.5944 (8)	350
O	0.2005 (5)	0.4244 (10)	0.5253 (8)	626
C(1)	0.2792 (7)	0.7592 (15)	0.7873 (12)	607
C(2)	0.2231 (8)	0.7273 (13)	0.8068 (11)	570
C(3)	0.1875 (7)	0.7428 (15)	0.7205 (11)	560
C(4)	0.2242 (8)	0.7843 (14)	0.6466 (12)	591
C(5)	0.2785 (8)	0.7908 (13)	0.6872 (11)	547
P(1)	0.34355 (14)	0.51112 (33)	0.66395 (23)	314
C(111)	0.4118 (6)	0.2909 (18)	0.7405 (10)	600
C(112)	0.4198 (8)	0.1603 (19)	0.7594 (11)	822
C(113)	0.3787 (10)	0.0757 (18)	0.7304 (14)	744
C(114)	0.3309 (8)	0.1194 (16)	0.6790 (12)	602
C(115)	0.3221 (6)	0.2477 (13)	0.6597 (9)	433
C(116)	0.3621 (5)	0.3415 (14)	0.6904 (8)	363
C(121)	0.3279 (6)	0.6055 (14)	0.4681 (10)	444
C(122)	0.3434 (7)	0.6231 (16)	0.3712 (10)	569
C(123)	0.3886 (8)	0.5665 (15)	0.3446 (11)	599
C(124)	0.4221 (8)	0.4841 (20)	0.4061 (11)	758
C(125)	0.4069 (7)	0.4612 (16)	0.5055 (11)	588
C(126)	0.3586 (6)	0.5232 (13)	0.5352 (10)	417
C(131)	0.4128 (6)	0.5933 (14)	0.8305 (11)	513
C(132)	0.4550 (7)	0.6703 (15)	0.8834 (12)	621
C(133)	0.4847 (7)	0.7545 (16)	0.8309 (15)	658
C(134)	0.4728 (6)	0.7703 (14)	0.7343 (13)	553
C(135)	0.4307 (6)	0.6988 (14)	0.6836 (11)	481
C(136)	0.3993 (6)	0.6096 (13)	0.7305 (10)	409
P(2)	0.24178 (14)	0.40699 (35)	0.81343 (23)	359
C(211)	0.3309 (6)	0.3172 (15)	0.9405 (11)	521
C(212)	0.3741 (6)	0.3191 (17)	1.0167 (10)	546
C(213)	0.3797 (8)	0.4241 (19)	1.0769 (12)	663
C(214)	0.3434 (8)	0.5275 (20)	1.0620 (11)	694
C(215)	0.3004 (7)	0.5296 (16)	0.9871 (11)	566
C(216)	0.2933 (7)	0.4215 (12)	0.9202 (10)	419
C(221)	0.1654 (7)	0.4298 (13)	0.9628 (11)	558
C(222)	0.1116 (8)	0.4318 (16)	0.9929 (13)	698
C(223)	0.0653 (8)	0.4335 (17)	0.9238 (15)	797
C(224)	0.0734 (7)	0.4399 (15)	0.8263 (15)	711
C(225)	0.1258 (7)	0.4385 (14)	0.7983 (11)	555
C(226)	0.1751 (6)	0.4325 (12)	0.8637 (9)	389

Table IV. Bond Distances in **4a** (Å)

Re-P(2)	2.461 (3)	C(221)-C(222)	1.385 (27)
Re-P(1)	2.358 (3)	C(222)-C(223)	1.376 (26)
Re-N	1.738 (10)	C(223)-C(224)	1.357 (29)
Re-C(1)	2.287 (16)	C(224)-C(225)	1.343 (24)
Re-C(2)	2.316 (16)	C(225)-C(226)	1.404 (20)
Re-C(3)	2.321 (16)	C(226)-C(221)	1.388 (20)
Re-C(4)	2.249 (15)	C(111)-C(112)	1.371 (27)
Re-C(5)	2.234 (14)	C(112)-C(113)	1.339 (29)
P(2)-C(216)	1.813 (14)	C(113)-C(114)	1.352 (28)
P(2)-C(226)	1.811 (15)	C(114)-C(115)	1.351 (21)
N-O	1.208 (15)	C(115)-C(116)	1.388 (19)
P(1)-C(116)	1.818 (14)	C(116)-C(111)	1.407 (19)
P(1)-C(126)	1.823 (14)	C(121)-C(122)	1.413 (21)
P(1)-C(136)	1.835 (14)	C(122)-C(123)	1.305 (26)
C(1)-C(2)	1.428 (25)	C(123)-C(124)	1.384 (24)
C(2)-C(3)	1.385 (21)	C(124)-C(125)	1.450 (23)
C(3)-C(4)	1.457 (24)	C(125)-C(126)	1.408 (22)
C(4)-C(5)	1.360 (25)	C(126)-C(121)	1.393 (19)
C(5)-C(1)	1.394 (22)	C(131)-C(132)	1.416 (21)
C(211)-C(212)	1.386 (19)	C(132)-C(133)	1.361 (24)
C(212)-C(213)	1.348 (24)	C(133)-C(134)	1.323 (26)
C(213)-C(214)	1.370 (27)	C(134)-C(135)	1.373 (20)
C(214)-C(215)	1.370 (22)	C(135)-C(136)	1.375 (20)
C(215)-C(216)	1.430 (20)	C(136)-C(131)	1.373 (19)
C(216)-C(211)	1.404 (20)		

um-fragment HOMO/ PH_2 lone-pair overlap and also corresponds to the $\text{Re}-\text{CH}_3$ maximum at $235\text{-}240^\circ$.

The θ dependence of the HOMO energy of $(\eta^5\text{-C}_5\text{H}_5)\text{Re}(\text{NO})(\text{PH}_3)(\text{PH}_2)$ closely follows the θ dependence of E_{total} (Figure 5). This strongly suggests that HOMO stability is the most

Table V. Bond Angles in **4a** (Deg)

P(1)-Re-P(2)	92.5 (1)	C(126)-C(121)-C(122)	121.1 (14)
P(1)-Re-N	91.5 (4)	C(121)-C(122)-C(123)	120.0 (14)
P(2)-Re-N	92.5 (4)	C(122)-C(123)-C(124)	123.2 (16)
Re-N-O	177.9 (10)	C(123)-C(124)-C(125)	118.5 (16)
Re-P(2)-C(216)	111.7 (5)	C(124)-C(125)-C(126)	118.7 (14)
Re-P(2)-C(226)	107.5 (4)	C(125)-C(126)-C(127)	118.5 (13)
C(226)-P(2)-C(216)	103.8 (6)	C(136)-C(131)-C(132)	121.3 (16)
Re-P(1)-C(116)	118.0 (4)	C(131)-C(132)-C(133)	117.8 (15)
Re-P(1)-C(126)	114.0 (5)	C(132)-C(133)-C(134)	121.7 (15)
Re-P(1)-C(136)	112.9 (5)	C(212)-C(213)-C(214)	120.2 (15)
C(126)-P(1)-C(116)	100.8 (6)	C(213)-C(214)-C(215)	122.5 (17)
C(136)-P(1)-C(116)	106.1 (6)	C(214)-C(215)-C(216)	119.5 (15)
C(136)-P(1)-C(126)	103.4 (6)	C(215)-C(216)-C(211)	115.5 (13)
C(5)-C(1)-C(2)	108.2 (14)	C(226)-C(221)-C(222)	122.3 (15)
C(1)-C(2)-C(3)	108.9 (14)	C(221)-C(222)-C(223)	120.3 (17)
C(2)-C(3)-C(4)	104.9 (14)	C(222)-C(223)-C(224)	118.9 (18)
C(3)-C(4)-C(5)	110.4 (14)	C(223)-C(224)-C(225)	120.1 (16)
C(4)-C(5)-C(1)	107.6 (16)	C(224)-C(225)-C(226)	124.6 (15)
C(116)-C(111)-C(112)	123.0 (15)	C(225)-C(226)-C(221)	113.8 (14)
C(111)-C(112)-C(113)	119.4 (17)	P(2)-C(216)-C(211)	117.6 (10)
C(112)-C(113)-C(114)	119.7 (17)	P(2)-C(216)-C(215)	126.9 (11)
C(113)-C(114)-C(115)	121.8 (16)	P(2)-C(226)-C(221)	126.9 (11)
C(114)-C(115)-C(116)	121.7 (14)	P(2)-C(226)-C(225)	118.7 (11)
C(133)-C(134)-C(135)	120.4 (15)	P(1)-C(116)-C(111)	128.6 (11)
C(134)-C(135)-C(136)	121.7 (14)	P(1)-C(116)-C(115)	117.0 (10)
C(135)-C(136)-C(131)	116.9 (13)	P(1)-C(126)-C(121)	121.8 (11)
C(216)-C(211)-C(212)	123.3 (16)	P(1)-C(126)-C(125)	119.2 (10)
C(211)-C(212)-C(213)	119.0 (15)	P(1)-C(136)-C(131)	120.5 (11)
C(115)-C(116)-C(111)	114.4 (13)	P(1)-C(136)-C(135)	122.5 (10)

Table VI. Atomic Coordinates of Non-Hydrogen Atoms in $(\eta^5\text{-C}_5\text{H}_5)\text{Re}(\text{NO})(\text{PPh}_3)(\text{P}(t\text{-Bu})_2)$ (**4d**)

atom	x	y	z	$U(\text{eq}/\text{iso}) \times 10^4$
Re	0.09800 (7)	0.36408 (6)	0.28179 (5)	256 (6)
P(2)	0.35027 (45)	0.34877 (37)	0.27421 (32)	360 (37)
P(1)	0.14724 (42)	0.15926 (33)	0.24140 (29)	290 (33)
O	0.1285 (13)	0.2910 (10)	0.5009 (8)	565 (12)
N	0.1177 (12)	0.3205 (10)	0.4095 (9)	290 (3)
C(1)	0.3440 (19)	0.4982 (17)	0.3248 (14)	546 (18)
C(2)	0.2566 (20)	0.5155 (16)	0.4282 (14)	550 (18)
C(3)	0.2824 (20)	0.6180 (15)	0.2548 (16)	626 (19)
C(4)	0.4973 (20)	0.4728 (19)	0.3503 (16)	700 (22)
C(5)	0.4444 (17)	0.3243 (15)	0.1400 (13)	429 (16)
C(6)	0.5149 (22)	0.1788 (17)	0.1324 (17)	760 (22)
C(7)	0.5732 (22)	0.3570 (20)	0.1311 (17)	775 (24)
C(8)	0.3500 (23)	0.3879 (20)	0.0489 (14)	757 (22)
C(10)	-0.1330 (16)	0.5073 (15)	0.2873 (14)	467 (15)
C(11)	-0.0479 (17)	0.5786 (13)	0.2623 (13)	431 (15)
C(12)	0.0272 (18)	0.5413 (13)	0.1648 (12)	399 (15)
C(13)	-0.0108 (17)	0.4519 (14)	0.1294 (11)	409 (15)
C(14)	-0.1127 (16)	0.4333 (15)	0.2022 (14)	449 (16)
C(20)	0.3208 (16)	0.0279 (13)	0.2622 (12)	333 (14)
C(21)	0.3915 (17)	0.0306 (14)	0.3452 (13)	434 (15)
C(22)	0.5186 (19)	-0.0704 (17)	0.3713 (15)	618 (19)
C(23)	0.5751 (20)	-0.1744 (16)	0.3136 (16)	604 (19)
C(24)	0.5062 (20)	-0.1803 (16)	0.2286 (16)	593 (19)
C(25)	0.3777 (19)	-0.0769 (14)	0.2020 (13)	501 (17)
C(30)	0.0276 (16)	0.1024 (13)	0.3166 (10)	306 (4)
C(31)	-0.0933 (18)	0.1804 (15)	0.3686 (14)	487 (16)
C(32)	-0.1882 (21)	0.1374 (19)	0.4204 (17)	718 (22)
C(33)	-0.1578 (20)	0.0127 (18)	0.4210 (15)	582 (20)
C(34)	-0.0346 (24)	-0.0667 (17)	0.3705 (15)	634 (21)
C(35)	0.0598 (19)	-0.0255 (14)	0.3200 (13)	502 (17)
C(40)	0.1057 (17)	0.1480 (12)	0.1098 (11)	330 (14)
C(41)	-0.0284 (20)	0.1566 (15)	0.0874 (13)	496 (17)
C(42)	-0.0591 (21)	0.1567 (16)	-0.0127 (15)	525 (19)
C(43)	0.0332 (28)	0.1477 (17)	-0.0931 (15)	667 (23)
C(44)	0.1701 (26)	0.1361 (16)	-0.0726 (14)	652 (22)
C(45)	0.2071 (19)	0.1366 (16)	0.0287 (13)	514 (18)

important contribution to the $\text{Re}-\text{PH}_2$ conformational preference, in accordance with Walsh's rule.³⁰ The appearance of substantial PH_2 lone-pair character in the HOMO as conformations approach energy maxima indicates that HOMO destabilization results from unfavorable rhenium-fragment HOMO/ PH_2 lone-pair overlap.

(30) Albright, T. A.; Burdett, J. K.; Whangbo, M.-H. *Orbital Interactions in Chemistry*; Wiley-Interscience: New York, 1985; p 94.

Table VII. Bond Distances in **4d** (Å)

Re-P(2)	2.526 (4)	C(11)-C(12)	1.432 (22)
Re-P(1)	2.357 (4)	C(12)-C(13)	1.400 (21)
Re-N	1.709 (11)	C(13)-C(14)	1.439 (21)
Re-C(10)	2.258 (15)	C(20)-C(21)	1.363 (21)
Re-C(14)	2.274 (16)	C(20)-C(25)	1.400 (21)
Re-C(13)	2.311 (14)	C(21)-C(22)	1.390 (22)
Re-C(11)	2.346 (13)	C(22)-C(23)	1.373 (25)
Re-C(12)	2.382 (14)	C(23)-C(24)	1.385 (26)
P(2)-C(5)	1.914 (16)	C(24)-C(25)	1.414 (23)
P(2)-C(1)	1.916 (17)	C(30)-C(31)	1.359 (21)
P(1)-C(20)	1.825 (15)	C(30)-C(35)	1.409 (20)
P(1)-C(40)	1.829 (15)	C(31)-C(32)	1.398 (24)
P(1)-C(30)	1.837 (15)	C(32)-C(33)	1.377 (26)
N-O	1.218 (14)	C(33)-C(34)	1.369 (25)
C(1)-C(4)	1.537 (24)	C(34)-C(35)	1.373 (24)
C(1)-C(2)	1.540 (24)	C(40)-C(41)	1.397 (23)
C(1)-C(3)	1.545 (25)	C(40)-C(45)	1.401 (21)
C(5)-C(7)	1.532 (24)	C(41)-C(42)	1.368 (23)
C(5)-C(8)	1.532 (25)	C(42)-C(43)	1.340 (26)
C(5)-C(6)	1.571 (23)	C(43)-C(44)	1.405 (29)
C(10)-C(14)	1.415 (24)	C(44)-C(45)	1.406 (25)
C(10)-C(11)	1.467 (23)		

Table VIII. Bond Angles in **4d** (Deg)

P(1)-Re-P(2)	100.0 (1)	C(14)-C(10)-C(11)	106.4 (14)
P(1)-Re-N	90.9 (4)	C(12)-C(11)-C(10)	108.3 (14)
P(2)-Re-N	87.6 (4)	C(13)-C(12)-C(11)	107.5 (14)
Re-N-O	178.6 (11)	C(12)-C(13)-C(14)	109.3 (14)
Re-P(2)-C(1)	108.7 (6)	C(10)-C(14)-C(13)	108.4 (15)
Re-P(2)-C(5)	114.7 (5)	C(21)-C(20)-C(25)	119.6 (14)
C(1)-P(2)-C(5)	108.7 (8)	C(21)-C(20)-P(1)	117.0 (12)
C(10)-Re-P(2)	140.8 (5)	C(25)-C(20)-P(1)	123.3 (13)
C(11)-Re-P(2)	104.1 (4)	C(20)-C(21)-C(22)	120.5 (16)
C(12)-Re-P(2)	90.2 (4)	C(23)-C(22)-C(21)	120.6 (18)
C(13)-Re-P(2)	110.4 (4)	C(22)-C(23)-C(24)	120.4 (17)
C(14)-Re-P(2)	146.8 (4)	C(23)-C(24)-C(25)	118.8 (16)
C(20)-P(1)-C(40)	105.5 (7)	C(20)-C(25)-C(24)	120.1 (17)
C(20)-P(1)-C(30)	100.3 (6)	C(31)-C(30)-C(35)	118.3 (14)
C(20)-P(1)-Re	122.4 (5)	C(31)-C(30)-P(1)	122.0 (11)
C(40)-P(1)-C(30)	101.3 (7)	C(35)-C(30)-P(1)	119.6 (11)
C(40)-P(1)-Re	113.2 (4)	C(30)-C(31)-C(32)	121.6 (16)
C(30)-P(1)-Re	111.4 (5)	C(33)-C(32)-C(31)	119.7 (17)
C(4)-C(1)-C(2)	106.4 (15)	C(34)-C(33)-C(32)	119.0 (16)
C(4)-C(1)-C(3)	108.8 (16)	C(33)-C(34)-C(35)	121.8 (16)
C(4)-C(1)-P(2)	107.9 (12)	C(34)-C(35)-C(30)	119.6 (16)
C(2)-C(1)-C(3)	110.8 (15)	C(41)-C(40)-C(45)	118.8 (15)
C(2)-C(1)-P(2)	104.8 (12)	C(41)-C(40)-P(1)	121.3 (12)
C(3)-C(1)-P(2)	117.5 (12)	C(45)-C(40)-P(1)	119.8 (13)
C(7)-C(5)-C(8)	108.6 (16)	C(42)-C(41)-C(40)	119.6 (17)
C(7)-C(5)-C(6)	103.6 (14)	C(43)-C(42)-C(41)	124.0 (19)
C(7)-C(5)-P(2)	112.9 (12)	C(42)-C(43)-C(44)	117.6 (18)
C(8)-C(5)-C(6)	110.7 (16)	C(43)-C(44)-C(45)	120.9 (18)
C(8)-C(5)-P(2)	116.8 (12)	C(40)-C(45)-C(44)	119.1 (17)
C(6)-C(5)-P(2)	103.3 (11)		

Table IX. Phosphorus Inversion Barriers Determined from NMR Coalescence Temperatures

compd	temp, K	ΔG^\ddagger , kcal/mol
4b	264	13.0 \pm 0.1
4b	255	13.3 \pm 0.2
4c	308	14.7 \pm 0.1
4c	312	14.9 \pm 0.1
4d	266	12.6 \pm 0.1

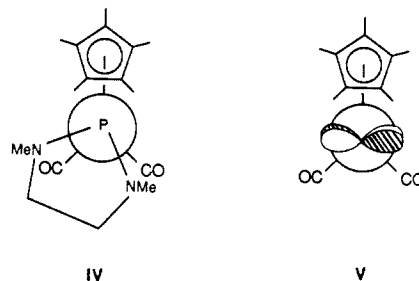
Furthermore, the possibility that the preferred conformations result from favorable overlap between a rhenium-fragment acceptor orbital and the PH_2 lone pair is eliminated by the θ independence of the accessible LUMOs (Figure 5). It is therefore clear that conformation is influenced by avoided overlap, thus establishing a firm theoretical basis for the existence of a transition-metal "gauche effect".

The relative energies of the two Re-PH₂ minima in Figure 4 are quite sensitive to steric effects and reverse when PH₃ is replaced by PMe₃.²⁶ Accordingly, conformations corresponding to the θ

= 150° minimum are found in the solid state of **4a** and **4d**. Since **4a** and **4d** have quite different phosphido substituents, we believe it is unlikely that both would crystallize in higher energy Re-PR₂ conformations. Also, it is now recognized that the region between the NO and PPh₃ ligands is the sterically most congested in these and related complexes,^{16b,31,32} and thus any phosphido substituent should destabilize the $\theta = 320^\circ$ conformer. Importantly, Seeman and Davies have also noted significant differences in calculated relative energies of metal-ligand conformers when the model ligand PH₃ is replaced by a bulkier ligand.³¹

Finally, we wish to emphasize that we by no means consider steric Re-PR₂ conformation-determining factors to be negligible in **4a-d**.³³ The above analysis is intended to establish the existence, not necessarily the dominance, of a "gauche effect". Toward this end, efforts are being directed at the preparation of carbonyl-substituted complexes $[(\eta^5\text{-C}_5\text{H}_5)\text{Re}(\text{NO})(\text{CO})(\text{L})]^{n+}$ (L = PR₂, NR₂, SR₂).³⁴ Here, the metal-fragment HOMO is analogous to that shown in I,^{4c} but one of the ancillary ligands is much smaller, and the isosteric NO and CO ligands create an effective mirror plane.

At this time, only a limited number of other pyramidal phosphido complexes can be analyzed for a "gauche effect". A view of the solid-state structure of $(\eta^5\text{-C}_5\text{Me}_5)\text{Fe}(\text{CO})_2(\text{PN}(\text{CH}_3)_2\text{CH}_2\text{CH}_2\text{NCH}_3)$ is given in IV.^{13c} Paine reports the OC-Fe-P-N



torsion angles as ca. 24°. The PPH₂ ligand adopts a similar conformation in $(\eta^5\text{-C}_5\text{Me}_5)\text{Fe}(\text{CO})_2(\text{PPh}_2)$.^{13c} The HOMO of the iron fragment $[(\eta^5\text{-C}_5\text{Me}_5)\text{Fe}(\text{CO})_2]^+$ is the d-type orbital shown in V and is nearly orthogonal to the phosphido lone pair in IV. However, the second HOMO of this iron fragment is an orthogonal d-type orbital that lies in the molecular symmetry plane and is close in energy to the HOMO.^{4b,c,35} Thus, Fe-PX₂ conformational analysis in these complexes may be complicated by phosphido lone-pair avoided overlap with two metal orbitals.

3. Phosphorus Inversion. Exchange of the diastereotopic aryl- and alkylphosphido substituents in **4a-d** requires two molecular actions: phosphido phosphorus inversion and Re-PR₂ bond rotation. The interplay of these events in dynamic processes of other "gauche effect" molecules has been considered in detail by others.¹¹ In principle, our 12.6–14.9 kcal/mol barriers (Table IX) are upper limits to the actual phosphorus-atom inversion barrier. However, we have no evidence at present for extraordinary Re-PR₂ rotational barriers in this system.

(31) (a) Seeman, J. I.; Davies, S. G. *J. Am. Chem. Soc.* **1985**, *107*, 6522. (b) Seeman, J. I. *Pure Appl. Chem.* **1987**, *59*, 1661.

(32) Hunter, B. K.; Baird, M. C. *Organometallics* **1985**, *4*, 1481.

(33) In essence, complexes **4a** and **4d** exhibit Re-PR₂ conformational minima that are also close to what would be expected from steric considerations alone, so the relative importance of these two conformation-determining factors cannot be readily assessed. Consider the X-ray structure of the secondary alkyl complex $(SS,RR)-(\eta^5\text{-C}_5\text{H}_5)\text{Re}(\text{NO})(\text{PPh}_3)(\text{CH}(\text{CH}_2\text{Ph})\text{Ph})$,^{16a} in which the phosphido phosphorus of **4a** is replaced by a CH moiety, and one of the phenyl groups by a benzyl group. Here, steric conformation-determining factors should be magnified, since the Re-C_α bond (2.215 (4) Å) is much shorter than the Re-PPh₂ bond of **4a** (2.461 (3) Å). The Re-C_α conformation found is much like the Re-PR₂ conformations of **4a** and **4d**, with a H-C_α-Re-PPh₃ torsion angle of 54.6°.^{31a} This compares with 59.7° for the analogous angle involving the lone pair in **4a**. While we believe this ca. 5° difference is likely significant, experiments with compounds where steric and electronic effects give differing conformational predictions are in progress.

(34) Quirós, N., unpublished results, University of Utah.

(35) Riley, P. E.; Davis, R. E.; Allison, N. T.; Jones, W. M. *Inorg. Chem.* **1982**, *21*, 1321.

Typically, inversion barriers for trialkylphosphines are greater than 30 kcal/mol.^{36,37} Low barriers have been previously observed in silyl and acyl phosphines such as $\text{PhP}(\text{SiHMe}_2)_2$ (12 kcal/mol) and $\text{PhP}(\text{CO}(i\text{-Pr}))_2$ (12 kcal/mol) and substituted phospholes (15–16 kcal/mol).^{36a,b} Malisch has reported an inversion barrier of 14.4 kcal/mol for the pyramidal phosphido ligand in $(\eta^5\text{-C}_5\text{H}_5)\text{W}(\text{CO})_2(\text{PMe}_3)(\text{P}(i\text{-Pr})_2)$.^{14b} We observe an 11.5 kcal/mol barrier for phosphido ligand inversion in phenylphosphido complex $(\eta^5\text{-C}_5\text{H}_5)\text{Re}(\text{NO})(\text{PPh}_3)(\text{PPhH})$.^{19b,38} Hence, phosphorus inversion barriers in pyramidal metal phosphido complexes are among the lowest known.

While the low phosphorus inversion barriers in **4a–d** are not easily attributed to a single property, several possible contributing factors can be identified.³⁹ Generally, inversion barriers are decreased by substituents that are good σ donors or good π acceptors.^{37a} Furthermore, larger bond angles about a pyramidal center make the planar transition state easier to reach.^{37a} The electropositive rhenium substituent and large angles about phosphorus in **4a–d** should thus lower the inversion barriers. However, substituents that are good π donors, as the $(\eta^5\text{-C}_5\text{H}_5)\text{Re}(\text{NO})(\text{PPh}_3)^+$ fragment, generally raise inversion barriers. Another possible contribution would result from any π -accepting capabilities of the rhenium moiety. However, the calculations on model complex $(\eta^5\text{-C}_5\text{H}_5)\text{Re}(\text{NO})(\text{PH}_3)(\text{PH}_2)$ do not show any favorable interactions of the PH_2 lone pair with unoccupied metal orbitals. An alternative would be to invoke $\eta^5\text{-C}_5\text{H}_5$ slippage or NO bending (which would create new metal acceptor orbitals) prior to or concurrently with phosphorus planarization. However, we recently measured sulfur inversion barriers in sulfide complexes $[(\eta^5\text{-C}_5\text{H}_5)\text{Re}(\text{NO})(\text{L})(\text{SMe}_2)]^+\text{TfO}^-$, where $\text{L} = \text{CO}$ and PPh_3 .³⁴ Higher inversion barriers are found with $\text{L} = \text{CO}$,^{39a} although the rhenium π -accepting capabilities should be greater.^{4b,c}

4. Phosphido Ligand Reactions. Compounds that exhibit the gauche effect often show enhanced solution-phase nucleophilicity (" α effect").¹² The origin and nature of this effect are poorly understood. Others have previously demonstrated the nucleophilicity of metal phosphido ligands toward common electrophiles such as alkyl iodides, halogens, and mineral acids.^{13a,14b,f,k,m} The ready reaction of **4a** and CH_2Cl_2 (Scheme II) dramatically illustrates the exceptional nucleophilicity of the phosphido ligands in **4a–d**. No reaction occurs between PPh_3 and CH_2Cl_2 over an extended period,⁴⁰ and CH_2Cl_2 is 10^{-3} less reactive than CH_3Cl toward nucleophilic substitution (50 °C, acetone).⁴¹ Recently, the very bulky triarylphosphine $[2,4,6\text{-(CH}_3\text{O)}_3\text{C}_6\text{H}_2]_3\text{P}$ has been shown to similarly react with CH_2Cl_2 .⁴⁰

The air oxidation of **4a** (Scheme II) occurs much more readily than that of PPh_3 , which parallels the nucleophilicity order noted above. There are two previous reports of the oxidation of phosphido ligands: the reaction of $(\eta^5\text{-C}_5\text{H}_5)\text{Fe}(\text{CO})_2(\text{P}(\text{CF}_3)_2)$ with NO to give $(\eta^5\text{-C}_5\text{H}_5)\text{Fe}(\text{CO})_2(\text{P}(\text{=O})(\text{CF}_3)_2)$,^{14d} and the reaction of $\text{Ir}(\text{CO})(\text{Cl})_2(\text{PEt}_3)_2(\text{PCl}_2)$ with O_2 or N_2O_4 to give $\text{Ir}(\text{CO})(\text{Cl})_2(\text{PEt}_3)_2(\text{P}(\text{=O})\text{Cl}_2)$.^{13b} Phosphine oxides typically show strong IR $\nu_{\text{P=O}}$ in the 1200–1140- cm^{-1} range.⁴² However, **6a** and

6d exhibit lower intensity absorbances in the 1113–1061- cm^{-1} range. We speculate that these bands are $\nu_{\text{P=O}}$, with the shift to lower frequency reflecting a contribution by a $\text{Re}^+=\text{PR}_2\text{O}^-$ resonance form to the ground state. Similar shifts in IR $\nu_{\text{C=O}}$ are observed in acyl complexes $(\eta^5\text{-C}_5\text{H}_5)\text{Re}(\text{NO})(\text{PPh}_3)(\text{COR})$.¹⁷

5. Conclusions. We have established a sound theoretical basis for the existence of a transition-metal "gauche effect" and have described a class of compounds that exhibit several properties consistent with this phenomenon. Since there are numerous transition-metal complexes that contain lone pairs on ligating atoms ($-\text{PR}_2$, $-\text{NR}_2$, $-\text{SR}_2$, $-\text{OR}$, $-\text{SR}$, etc.), this concept, like that of back-bonding, has ramifications for the physical and chemical properties of many compounds. We further predict that these compounds will show enhancements in nucleophilicity over model organic compounds (" α effect") and unusual configurational properties. This concept should ultimately prove useful in the construction of inorganic molecules with carefully designed conformational properties, such as asymmetric catalysts, selective chelating agents, and synthetic enzymes. Further studies on the transition-metal "gauche effect" are in progress.

Experimental Section

General Data. All reactions were carried out under a dry N_2 atmosphere. IR spectra were recorded on a Perkin-Elmer 1500 (FT) spectrometer. All ^1H and ^{13}C NMR spectra were recorded on Varian 300-MHz spectrometers and were referenced to internal Me_4Si unless noted. All ^{31}P NMR spectra were recorded on Varian FT-80A and 300-MHz spectrometers and were referenced to external H_3PO_4 . Mass and UV/visible spectra were obtained on VG 770 and Cary 17D spectrometers, respectively. Optical rotations were measured on a Perkin-Elmer 141 spectropolarimeter. Microanalyses were conducted by Galbraith and Schwarzkopf Laboratories. Melting points were determined in evacuated capillaries and were not corrected.

Solvents were distilled (CH_2Cl_2 and CHCl_3 , from P_2O_5 ; benzene, ether, and THF, from Na/benzophenone; hexane and heptane, from sodium; pentane, from LiAlH_4) and freeze-thaw-pump degassed (three times) before use. Deuterated solvents were trap-to-trap distilled from the following drying agents: CD_2Cl_2 and CDCl_3 , P_2O_5 ; THF- d_8 , benzene- d_6 , and toluene- d_8 , CaH_2 .

Reagents were obtained as follows: PPh_2H (Strem), distilled before use; $\text{P}(p\text{-Tol})_2\text{H}$, prepared from $\text{P}(p\text{-Tol})_3$ by a literature procedure⁴⁴ and distilled at 10^{-3} Torr; PEt_2H (Strem), distilled before use; $\text{P}(t\text{-Bu})_2\text{H}$, prepared from $\text{P}(t\text{-Bu})_2\text{Cl}$ (Strem) by a literature procedure⁴⁵ and distilled before use; $t\text{-BuO}^-\text{K}^+$ (Aldrich), sublimed before use; PhIO , prepared from idosobenzene diacetate (Aldrich) by a literature procedure.⁴⁶

Preparation of $[(\eta^5\text{-C}_5\text{H}_5)\text{Re}(\text{NO})(\text{PPh}_3)(\text{PPh}_2\text{H})]^+\text{TsO}^-$ (2a-TsO**).** A Schlenk flask was charged with $(\eta^5\text{-C}_5\text{H}_5)\text{Re}(\text{NO})(\text{PPh}_3)(\text{OTs})$ (**1**);²⁰ 2.50 g, 3.50 mmol), PPh_2H (1.22 mL, 1.31 g, 7.00 mmol), CH_2Cl_2 (50 mL), and a stir bar. The solution was stirred for 2 days, after which it was concentrated in vacuo to ca. 25 mL. Addition to ether gave a precipitate that was collected by filtration, washed with ether, and air-dried to give **2a-TsO** as a yellow powder (2.95 g, 3.27 mmol, 94%). Crystallization from CHCl_3 /ether gave yellow crystals that were dried in vacuo, mp 150–155 °C dec. Anal. Calcd for $\text{C}_{42}\text{H}_{38}\text{NO}_4\text{P}_2\text{ReS}$: C, 55.99; H, 4.25. Found: C, 55.90; H, 4.24.

Preparation of $[(\eta^5\text{-C}_5\text{H}_5)\text{Re}(\text{NO})(\text{PPh}_3)(\text{P}(p\text{-Tol})_2\text{H})]^+\text{TsO}^-$ (2b-TsO**).** A Schlenk flask was charged with **1** (1.00 g, 1.40 mmol), $\text{P}(p\text{-Tol})_2\text{H}$ (0.61 mL, 0.60 g, 2.80 mmol), CH_2Cl_2 (50 mL), and a stir bar. The solution was stirred for 2 days, after which it was concentrated in vacuo to ca. 25 mL. Addition of ether gave a yellow oil that was washed with ether and redissolved in benzene. Then ether was added, and a solid slowly precipitated that was collected by filtration and dried in vacuo at 56 °C to give **2b-TsO** as an air-stable yellow powder (1.25 g, 1.35 mmol, 96%), mp 126–129 °C. Anal. Calcd for $\text{C}_{44}\text{H}_{42}\text{NO}_4\text{P}_2\text{ReS}$: C, 56.89; H, 4.56; S, 3.45. Found: C, 56.41; H, 4.44; S, 3.68.

Preparation of $[(\eta^5\text{-C}_5\text{H}_5)\text{Re}(\text{NO})(\text{PPh}_3)(\text{PEt}_2\text{H})]^+\text{TfO}^-$ (2c-TfO**).** A Schlenk flask was charged with $(\eta^5\text{-C}_5\text{H}_5)\text{Re}(\text{NO})(\text{PPh}_3)(\text{OTf})$ (**3**);²⁰ 1.16 g, 1.68 mmol), PEt_2H (0.24 mL, 0.19 g, 2.09 mmol), benzene (40 mL), and a stir bar. The solution was stirred for 4 h (changing from red

(36) (a) Rauk, A.; Allen, L. C.; Mislow, K. *Angew. Chem., Int. Ed. Engl.* **1970**, *9*, 400. (b) Mislow, K. *Trans. N.Y. Acad. Sci.* **1973**, *35*, Ser. 2, 227. (c) Macdonnel, G. D.; Berlin, K. D.; Baker, J. R.; Ealick, S. E.; van der Helm, D.; Marsi, K. L. *J. Am. Chem. Soc.* **1978**, *100*, 4535. (d) Schmidbaur, H.; Schier, A.; Lauteschläger, S.; Riede, J.; Müller, G. *Organometallics* **1984**, *3*, 1906.

(37) (a) Marynick, D. S.; Dixon, D. A. *J. Phys. Chem.* **1982**, *86*, 914. (b) Dixon, D. A.; Arduengo, A. J., III. *J. Am. Chem. Soc.* **1987**, *109*, 338.

(38) Zwick, B. D.; Buhro, W. E.; Arif, A. M.; Gladysz, J. A., manuscript in preparation.

(39) (a) In a series of thorough and elegant studies,^{39b,c} Abel and co-workers have demonstrated low sulfur inversion barriers in metal sulfide complexes $\text{L}_m\text{M-SRR}'$. For R, R' = alkyl, bulkier groups give lower inversion barriers.^{39c} Several trends in our inversion barriers (lower in **4d** than **4c**; higher upon replacement of PPh_3 by CO)³⁴ are likely also best accounted for by steric effects. (b) Abel, E. W.; Bhargava, S. K.; Orrell, K. G. *Prog. Inorg. Chem.* **1984**, *32*, 1. (c) Abel, E. W.; Moss, I.; Orrell, K. G.; Sik, V. J. *Organomet. Chem.* **1987**, *326*, 187.

(40) Wada, M.; Higashizaki, S. *J. Chem. Soc., Chem. Commun.* **1984**, 482.

(41) Alder, R. W.; Baker, R.; Brown, J. M. *Mechanism in Organic Chemistry*; Wiley: New York, 1971; p 198.

(42) (a) Lambert, J. B.; Shurvell, H. F.; Verbit, L.; Cooks, R. G.; Stout, G. H. *Organic Structural Analysis*; Macmillan: New York, 1976; p 280. (b) Silverstein, R. M.; Bassler, G. C.; Morill, T. C. *Spectrometric Identification of Organic Compounds*, 4th ed.; Wiley: New York, 1981; p 176.

(43) Mann, F. G.; Chaplin, E. J. *J. Chem. Soc.* **1937**, 527.

(44) Grim, S. O.; Yankowsky, A. W. *J. Org. Chem.* **1977**, *42*, 1236.

(45) Hoffman, H.; Schellenbeck, P. *Chem. Ber.* **1966**, *99*, 134.

(46) Saltzman, H.; Sharefkin, J. G. *Organic Synthesis*; Wiley: New York, 1973; Collect. Vol V, p 658.

to yellow), after which an aliquot was removed for a $^{31}\text{P}\{\text{H}\}$ NMR spectrum (complete reaction indicated). Addition of hexane (10 mL) precipitated a crude yellow product, which was collected by filtration and redissolved in a minimum of CH_2Cl_2 . Then ether was slowly added by vapor diffusion. Yellow plates formed, which were collected by filtration and dried in vacuo (56 °C) to give **2c-TfO⁻** (1.18 g, 1.51 mmol, 90%), mp 163–164 °C. Anal. Calcd for $\text{C}_{28}\text{H}_{31}\text{F}_3\text{NO}_4\text{P}_2\text{SRe}$: C, 42.97; H, 3.99; P, 7.91. Found: C, 42.61; H, 3.82; P, 7.79.

Preparation of $(\eta^5\text{-C}_5\text{H}_5)\text{Re}(\text{NO})(\text{PPh}_3)(\text{P}(t\text{-Bu})_2\text{H})\text{TfO}^-$ (2d-TfO⁻**).** An oven-dried Schlenk flask was charged with **3** (1.00 g, 1.44 mmol), $\text{P}(t\text{-Bu})_2\text{H}$ (0.63 g, 4.33 mmol), benzene (30 mL), and a stir bar and was fitted with a reflux condenser. The red solution was refluxed for 24 h, during which time a yellow powder precipitated. The powder was collected by filtration (1.02 g, 1.21 mmol, 84%), shown to be spectroscopically pure **2d-TfO⁻** (^1H , $^{31}\text{P}\{\text{H}\}$ NMR), and dissolved in CH_2Cl_2 . Ether was slowly added by vapor diffusion. Dark yellow needles formed, which were collected by filtration and dried in vacuo to give **2d-TfO⁻** (0.82 g, 0.98 mmol, 68%), mp 197–200 °C dec. Anal. Calcd for $\text{C}_{32}\text{H}_{39}\text{F}_3\text{NO}_4\text{P}_2\text{ReS}$: C, 45.83; H, 4.69. Found: C, 46.23; H, 4.89.

Preparation of $(\eta^5\text{-C}_5\text{H}_5)\text{Re}(\text{NO})(\text{PPh}_3)(\text{PPh}_2)$ (4a**).** A Schlenk flask was charged with **2a-TsO⁻** (2.95 g, 3.28 mmol), THF (150 mL), and a stir bar. Then $t\text{-BuO}^-\text{K}^+$ (0.405 g, 3.61 mmol) was added with stirring. After 3 h, the mixture was filtered. The filtrate was concentrated in vacuo to ca. 10 mL. Addition of ether yielded a precipitate that was collected by filtration, washed with ether, and dried in vacuo to give **4a** (2.38 g, 3.26 mmol, 99%) as an air-sensitive red-orange powder. Crystallization from benzene/hexane gave red crystals that were dried in vacuo, mp >220 °C. Mass spectrum (m/e , 15 eV): 262 (Ph_3P^+ , 100%), 183 (Ph_2P^+ , 83%), 108 (PhP^+ , 40%). UV (nm (ϵ), THF): 259 pk (15000), 266 sh (14000), 272 sh (12000), 320 pk (9400), 355 pk (8500), 424 sh (3100). Anal. Calcd for $\text{C}_{33}\text{H}_{30}\text{NOP}_2\text{Re}$: C, 57.68; H, 4.15. Found: C, 57.49; H, 4.17.

Preparation of $(\eta^5\text{-C}_5\text{H}_5)\text{Re}(\text{NO})(\text{PPh}_3)(\text{P}(p\text{-Tol})_2)$ (4b**).** A Schlenk flask was charged with **2b-TsO⁻** (1.00 g, 1.08 mmol), THF (50 mL), and a stir bar. Then $t\text{-BuO}^-\text{K}^+$ (0.133 g, 1.18 mmol) was added with stirring. After 5 h, the mixture was filtered. The filtrate was concentrated in vacuo to ca. 5 mL. Addition of ether yielded a precipitate that was collected by filtration and dried in vacuo to give **4b** (0.674 g, 0.892 mmol, 83%) as an air-sensitive orange powder. Crystallization from THF/hexane gave red crystals that were dried in vacuo (56 °C), mp 157–163 °C dec. Mass spectrum (m/e , 17 eV): 262 (Ph_3P^+ , 100%), 108 (PhP^+ , 8%), 8%. Anal. Calcd for $\text{C}_{37}\text{H}_{34}\text{NOP}_2\text{Re}$: C, 58.72; H, 4.53. Found: C, 58.34; H, 4.30.

Preparation of $(\eta^5\text{-C}_5\text{H}_5)\text{Re}(\text{NO})(\text{PPh}_3)(\text{PET}_3)$ (4c**).** A Schlenk flask was charged with **2c-TfO⁻** (0.40 g, 0.51 mmol), THF (30 mL), and a stir bar. Then $t\text{-BuO}^-\text{K}^+$ (0.063 g, 0.56 mmol) was added with stirring. After 5 min, the THF was removed in vacuo. The resulting orange residue was extracted with benzene, and the extract was filtered through Celite on a fritted funnel. Solvent was removed from the brilliant orange filtrate in vacuo to give spectroscopically pure (^1H , $^{31}\text{P}\{\text{H}\}$ NMR) **4c** (0.30 g, 0.47 mmol, 93%), which was then dissolved in a minimum of THF. Pentane was slowly added by vapor diffusion. Orange prisms formed (0.15 g, 0.24 mmol, 47%), which were collected by filtration and dried in vacuo (56 °C), mp 128–129 °C. UV (nm (ϵ), 1.33×10^{-4} M in THF): 246 sh (12200), 252 sh (10400), 258 sh (9250), 272 sh (6920), 308 sh (4740); $\epsilon = 1200$ at 400 nm. Anal. Calcd for $\text{C}_{27}\text{H}_{30}\text{NOP}_2\text{Re}$: C, 51.26; H, 4.78. Found: C, 51.30; H, 4.62.

Preparation of $(\eta^5\text{-C}_5\text{H}_5)\text{Re}(\text{NO})(\text{PPh}_3)(\text{P}(t\text{-Bu})_2)$ (4d**).** A Schlenk flask was charged with **2d-TfO⁻** (0.10 g, 0.14 mmol), THF (15 mL), and a stir bar. Then $t\text{-BuO}^-\text{K}^+$ (0.017 g, 0.15 mmol) was added with stirring. After 5 min, the THF was removed in vacuo. The resulting orange residue was extracted with benzene, and the extract was filtered through Celite on a fritted funnel. Solvent was removed from the filtrate in vacuo to give spectroscopically pure (^1H , $^{31}\text{P}\{\text{H}\}$ NMR) **4d** (0.076 g, 0.11 mmol, 79%), which was dissolved in a minimum of ether. Heptane was added until significant precipitation resulted. Ether was added until the solids dissolved, and the solution was placed in a -20 °C freezer. After 6 h, deep red prisms (0.038 g, 0.055 mmol, 39%) were collected by filtration and dried in vacuo (5 h), mp 152–156 °C dec. UV (nm (ϵ), 1.77×10^{-4} M in THF): 252 sh (11100), 257 sh (9100), 278 sh (6610), 285 sh (5590), 343 sh (4070); $\epsilon = 2150$ at 400 nm. Anal. Calcd for $\text{C}_{31}\text{H}_{38}\text{NOP}_2\text{Re}$: C, 54.06; H, 5.56. Found: C, 54.12; H, 5.73.

Preparation of $(\eta^5\text{-C}_5\text{H}_5)\text{Re}(\text{NO})(\text{PPh}_3)(\text{PPh}_2\text{CH}_2\text{Cl})\text{Cl}^- \cdot \text{CH}_2\text{Cl}_2$ (5a-Cl⁻·CH₂Cl₂**).** A Schlenk flask was charged with **4a** (0.200 g, 0.274 mmol), CH_2Cl_2 (15 mL), and a stir bar. The red solution was stirred and became yellow within 30 min. After ca. 3 h, stirring was ceased and ether was slowly added by vapor diffusion. This gave air-stable gold crystals of **5a-Cl⁻·CH₂Cl₂** (0.195 g, 0.217 mmol, 79%) that were collected by filtration, washed with ether, and dried in vacuo (56 °C), mp 160–161 °C dec. Anal. Calcd for $\text{C}_{37}\text{H}_{34}\text{Cl}_4\text{NOP}_2\text{Re}$: C, 49.45; H, 3.81; Cl,

15.78. Found: C, 49.32; H, 3.95; Cl, 16.14.

Preparation of $(\eta^5\text{-C}_5\text{H}_5)\text{Re}(\text{NO})(\text{PPh}_3)(\text{P}(=\text{O})\text{Ph}_2)$ (6a**).** A Schlenk flask was charged with **4a** (0.250 g, 0.343 mmol), THF (25 mL), and a stir bar. Then air (86 mL, 0.69 mmol of O_2) was bubbled through the solution by syringe. The sealed system was stirred for 21 h and then solvent was removed in vacuo. The resulting gold solid was dissolved in CH_2Cl_2 (5 mL). Hexane was added to a cloud point, and the mixture was filtered to remove a black substance. The filtrate was concentrated to ca. 1 mL in vacuo, and ether was added. The resulting precipitate was collected by filtration and dried in vacuo to give crude **6a** (0.181 g, ca. 70%) as a yellow powder of >90% purity by ^1H NMR. The powder was washed with THF (1 mL) and ether (ca. 5 mL) and dried in vacuo to give spectroscopically pure **6a** (0.114 g, 0.153 mmol, 45%). Crystallization from CH_2Cl_2 /hexane gave air-stable yellow-gold crystals that were dried in vacuo (56 °C), mp >220 °C. Mass spectrum (m/e , ^{187}Re , 15 eV): 745 (M^+ , 27%), 483 ($\text{M}^+ - \text{PPh}_3$, 100%), 467 ($\text{M}^+ - \text{PPh}_3\text{O}$, 16%), 359 ($(\eta^5\text{-C}_5\text{H}_5)\text{Re}(\text{NO})(\text{Ph})^+$, 18%), 262 (Ph_3P^+ , 23%). Anal. Calcd for $\text{C}_{35}\text{H}_{30}\text{NO}_2\text{P}_2\text{Re}$: C, 56.44; H, 4.06. Found: C, 56.29; H, 4.09. **B.** A Schlenk flask was charged with **4a** (0.250 g, 0.343 mmol), THF (10 mL), PhIO (0.079 g, 0.359 mmol), and a stir bar. The slurry was stirred for 3.5 h and turned brown-gold in the first few minutes. Workup as in the previous procedure gave crude **6a** in ca. 79% yield (0.201 g, >90% pure by ^1H NMR) and spectroscopically pure **6a** in 60% yield (0.154 g, 0.207 mmol).

Preparation of $(\eta^5\text{-C}_5\text{H}_5)\text{Re}(\text{NO})(\text{PPh}_3)(\text{P}(=\text{O})(t\text{-Bu})_2)$ (6d**).** A Schlenk flask was charged with **4d** (0.10 g, 0.14 mmol), THF (20 mL), PhIO (0.038 g, 0.17 mmol), and a stir bar. The resulting slurry was stirred for 4.5 h, at which time an aliquot was sampled by $^{31}\text{P}\{\text{H}\}$ NMR (complete reaction). The solvent was removed in vacuo and the residue was extracted with benzene. The extract was filtered through Celite, and the filtrate was concentrated. Hexane was slowly added by vapor diffusion. This gave bright orange prisms of **6d** (0.035 g, 0.050 mmol, 34%) that were collected by filtration and dried in vacuo (24 h), mp 221–223 °C dec. Anal. Calcd for $\text{C}_{31}\text{H}_{38}\text{NO}_2\text{PRe}$: C, 52.83; H, 5.43. Found: C, 52.88; H, 5.54.

Preparation of (-)-(S)-2b-TsO⁻**.** A Schlenk tube was charged with (-)-(S)-**1** (0.089 g, 0.124 mmol), $^{20}\text{P}(p\text{-Tol})_2\text{H}$ (0.134 mL, 0.133 g, 0.620 mmol), CH_2Cl_2 (1.5 mL), and a stir bar. The mixture was stirred for 16 h and then ether was slowly added by vapor diffusion. The resulting yellow oil was washed with ether and dried in vacuo to give spectroscopically pure (-)-(S)-**2b-TsO⁻** (0.094 g, 0.101 mmol, 82%). All attempts to crystallize this material gave oils. $[\alpha]_D^{25}$ $_{466} = -79^\circ$ (c 0.00082 g/mL, CH_2Cl_2). The IR and $^{31}\text{P}\{\text{H}\}$ NMR spectra were similar to those of the racemate.²⁶

Preparation of (+)-(S)-4b**.** A small vial was charged with (-)-(S)-**2b-TsO⁻** (0.094 g, 0.101 mmol), THF (5 mL), and a stir bar. Then $t\text{-BuO}^-\text{K}^+$ (0.012 g, 0.106 mmol) was added with stirring. After 2 h, the orange mixture was filtered. The filtrate was concentrated in a N_2 stream (<1 mL), and ether (3 mL) was added. The resulting precipitate was collected by filtration, washed with ether (2 mL), and dried in vacuo. This gave (+)-(S)-**4b** as an air-sensitive orange powder (0.058 g, 0.077 mmol, 76%), mp 122–126 °C dec. $[\alpha]_D^{25}$ $_{346} = 397^\circ$ (c 0.00073 g/mL, THF). The IR and $^{31}\text{P}\{\text{H}\}$ NMR spectra were very similar to those of the racemate.²⁶ As the solution was kept in the polarimeter cell, the specific rotation gradually diminished and then became negative (3 h, 381° ; 14 h, 229° ; 53 h, -421° ; $t_\infty = -580^\circ$). Concurrently, the solution turned from orange to dull yellow and maintained homogeneity. $^{31}\text{P}\{\text{H}\}$ NMR of presumed oxidation product (ppm, THF, -80 °C): 33.91 (br), 19.17 (d, $J_{\text{PP}} = 13.6$ Hz).

Variable-Temperature NMR. Experiments were conducted on Varian XL-300 or VXR-500 spectrometers. All coalescence temperatures were calibrated with either MeOH (low temperatures) or ethylene glycol (high temperatures) and are assumed to be accurate within ± 1 °C. Rate constants and ΔG^\ddagger were calculated by standard methods.⁴⁷ Additional data are given elsewhere.^{26,48}

X-ray Crystal Structure of **4a.** Crystals of **4a** were obtained as described above and X-ray data were collected on a Syntex P1 automated diffractometer as summarized in Table II. Lattice parameters (Table II) were determined from 15 centered reflections with 2θ between 20° and 25° . The data were corrected for Lorentz and polarization effects. Of 3063 unique reflections collected with $2\theta < 40^\circ$, 2653 with $I > 2.5\sigma(I)$ were used in the final refinement.

The structure was solved with the SHELX-76 program. Absorption corrections were applied and all non-hydrogen atoms were refined (by block matrix) with anisotropic thermal parameters. Anomalous dispersion corrections were applied throughout the refinement. The positions

(47) Sandström, J. *Dynamic NMR Spectrometry*; Academic: New York, 1982.

(48) Zwick, B. D. Ph.D. Thesis, University of Utah, 1987.

of the hydrogen atoms were calculated (C-H bond length 0.95 Å; idealized sp^3 geometry), and isotropic thermal parameters were assigned.

The "position" of the phosphido phosphorus lone pair was determined by locating a dummy hydrogen atom near P(2) with the idealized geometry for a bonded tertiary hydrogen. Torsion angles involving the lone pair were calculated from this dummy atom.

X-ray Crystal Structure of 4d. Crystals of **4d** were obtained as indicated above, and X-ray data were collected as described for **4a**. Lattice parameters (Table II) were determined from 15 centered reflections with 2θ between 16° and 29° . The data were corrected for Lorentz and polarization effects. During data collection, the intensity of individual standard reflections decreased 18–40%. The decrease for each reflection was reasonably linear, with a correlation coefficient of 0.92–0.94 for a least-squares fit. The crystal decomposed in the beam before an absorption correction could be determined. Of 4350 unique reflections collected with $2\theta < 50^\circ$, 3080 with $I > 2.5\sigma(I)$ were used in the final refinement.

The structure was solved by standard heavy-atom techniques with the UCLA Crystallographic Package.⁴⁹ Hydrogen atoms were generally placed in assigned positions, except on the methyl groups, where one hydrogen atom was located on the difference map and the others were assigned. Non-hydrogen atoms were refined with anisotropic thermal parameters, giving two atoms that refined to non-positive definite thermal parameters. The thermal parameters of these two atoms were made

isotropic and refined further. Anomalous dispersion corrections were applied throughout the refinement. The position of the phosphido phosphorus lone pair was calculated as described for **4a**. $\Delta/\sigma(\max)$: 0.016.

MO Calculations. Extended-Hückel MO calculations⁵⁰ were conducted with weighted H_{ij} formula. The rhenium and PH_3 phosphorus atoms of model compound $(\eta^5-C_5H_5)Re(NO)(PPh_3)(PH_2)$ were assigned idealized octahedral and tetrahedral geometries, respectively. The Re-PH₂ distance was set at 2.461 Å (Re-PAr₂ distance in **4a**), and the PH₂ phosphorus-hydrogen bond distances were set at 1.44 Å. The remaining bond lengths and H_{ii} and ζ parameters used were the same as employed previously.¹⁶ For each conformation θ , energy was minimized by rotating the Re-PH₃ bond (the same rotamer was optimum for all θ).

Acknowledgment. We thank the NSF for support of this research and A. T. Patton for assistance with the X-ray structure of **4d**.

Registry No. **1**, 92695-37-9; (-)-(S)-**1**, 110043-17-9; **2a-TsO⁻**, 96213-74-0; **2b-TsO⁻**, 113158-32-0; (-)-(S)-**2b-TsO⁻**, 113036-42-3; **2c-TfO⁻**, 113036-35-4; **2d-TfO⁻**, 113036-37-6; **3**, 92695-35-7; **4a**, 96213-75-1; **4b**, 98330-68-8; (+)-(S)-**4b**, 98461-38-2; **4c**, 113036-38-7; **4d**, 113036-39-8; **5a-Cl⁻**, 96213-76-2; **6a**, 96213-77-3; **6d**, 113036-43-4; $(\eta^5-C_5H_5)Re(NO)(PPh_3)(PH_2)$, 113036-40-1; P(*p*-Tol)₂H, 1017-60-3; PEt₂H, 627-49-6; PPh₂H, 829-85-6; P(*t*-Bu)₂H, 819-19-2.

Supplementary Material Available: Tables of hydrogen atom atomic coordinates and temperature factors for **4d** (3 pages); listing of structure factors for **4d** (15 pages). Ordering information is given on any current masthead page.

(50) (a) Hoffmann, R. *J. Chem. Phys.* **1963**, *39*, 1397. (b) Hoffmann, R.; Lipscomb, W. N. *Ibid.* **1962**, *36*, 2179, 3489; **1962**, *37*, 2872.

(49) Programs employed included CARESS (R. W. Broach, Argonne National Laboratory; CARESS incorporates features of PROFILE: Blessing, R. G.; Coppend, P.; Becker, P. *J. Appl. Crystallogr.* **1972**, *7*, 488), NORMAL, EXFFT, and SEARCH (all from the MULTAN-80 package, Peter Main, Department of Physics, University of York, York, England), and ORFLS (ORNL-TM-305), ORFFE (ORNL-TM-306), and ORTEP (ORNL-TM-5138). The least-squares refinement program, ORFLS, was modified to allow refinement of the coefficients of a scale function that was a quadratic function of exposure time: Ibers, J. A. *Acta Crystallogr., Sect. B* **1969**, *25*, 1667.

Redox-Promoted Linkage Isomerizations of Aldehydes and Ketones on Pentaammineosmium

W. Dean Harman, Mikiya Sekine, and Henry Taube*

Contribution from the Department of Chemistry, Stanford University, Stanford, California 94305. Received September 11, 1987

Abstract: Upon one-electron reduction, $[Os(NH_3)_5(\eta^1-(CH_3)_2CO)]^{3+}$ undergoes an $\eta^1 \rightarrow \eta^2$ isomerization at a specific rate of $6 \times 10^3 \text{ s}^{-1}$. Through the investigation of the homogeneous oxidation of $[Os(NH_3)_5(\eta^2-(CH_3)_2CO)]^{2+}$, a specific rate of 1.3 s^{-1} for the $\eta^2 \rightarrow \eta^1$ isomerization has also been determined. Thus, η^2 -coordination is preferred by 5.0 kcal mol⁻¹ for acetone bound to pentaammineosmium(II). The investigation has been extended to other aldehydes and ketones in order to explore the effects of strain, conjugation, and steric hindrance in the η^2 -bound ligand. Pentaammineosmium(II) was also found to interact with the aromatic portion of the phenones investigated. In these complexes, the metal coordinates η^2 to the arene, interrupting its aromaticity. Upon oxidation, an intramolecular isomerization occurs in which the Os(III) species adopt an η^1 -coordination at the carbonyl.

Recently, we reported the crystal structure of a novel pentaammineosmium(II) complex in which an acetone ligand is coordinated η^2 to the metal center.¹ Upon the one-electron oxidation of $[Os(NH_3)_5(\eta^2-(CH_3)_2CO)]^{2+}$ (**1**), a rapid linkage isomerization occurs in which the oxymetallocycle opens to yield a ketone terminally bound to osmium(III). When the resulting species $[Os(NH_3)_5(\eta^1-(CH_3)_2CO)]^{3+}$ is reduced, the acetone ligand reverts to η^2 -coordination. By investigation of the rates of these redox-coupled isomerizations, both by electrochemistry and by the study of the reactivity of **1** with homogeneous oxidants, we hoped to extract the driving forces and specific rates of isomerization for both di- and trivalent osmium complexes.

Although several η^2 -bound aldehyde and ketone complexes have been reported,² most are stable only at low temperature or when

the aldehyde or ketone contains electron-withdrawing groups; in no other case have changes in bonding mode attending a redox change been reported. We felt it worthwhile to take advantage of the special opportunity offered by our system because of the

(2) (a) Countryman, R.; Penfold, B. R. *J. Chem. Soc. D* **1971**, 1598. Countryman, R.; Penfold, B. R. *J. Cryst. Mol. Struct.* **1972**, *2*, 281. (b) Berke, H.; Bankhardt, W.; Huttner, G.; Seyerl, J. V.; Zsolnai, L. *Chem. Ber.* **1981**, *114*, 2754. (c) Kropp, K.; Skibbe, V.; Erker, G.; Krüger, C. *J. Am. Chem. Soc.* **1983**, *105*, 3353. Erker, G.; Rosenfeldt, F. *Tetrahedron Lett.* **1980**, *21*, 1637. (d) Clark, G. R.; Headfold, C. E. L.; Marsden, K.; Roper, W. R. *J. Organomet. Chem.* **1982**, *231*, 335–360. (e) Gambarotta, S.; Fioriani, C.; Chiesi-Villa, A.; Guastini, C. *J. Am. Chem. Soc.* **1985**, *107*, 2985–2986. (f) Buhro, W. E.; Georgiou, S.; Fernández, J. M.; Patton, A. T.; Strouse, C. E.; Gladysz, J. A. *Organometallics* **1986**, *5*, 956. (g) Fernández, J. M.; Emerson, K.; Larson, R. H.; Gladysz, J. A. *J. Am. Chem. Soc.* **1986**, *108*, 8268. (h) Tsou, T. T.; Huffman, J. C.; Kochi, J. K. *Inorg. Chem.* **1979**, *18*, 2311–2317. (i) Wood, C. D.; Schrock, R. R. *J. Am. Chem. Soc.* **1979**, *101*, 5421.

(1) Harman, W. D.; Fairlie, D. P.; Taube, H. *J. Am. Chem. Soc.* **1986**, *108*, 8223–8227.